AD NUMBER

AD917252

LIMITATION CHANGES

TO:

Approved for public release; distribution is unlimited.

FROM:

Distribution authorized to U.S. Gov't. agencies only; Administrative/Operational Use; 15 JUN 1973. Other requests shall be referred to Night Vision Laboratory, Fort Belvoir, VA 22060.

AUTHORITY

USAEC ltr, 2 May 1974

Semiannual Technical Report
Semiconductor-Insulator Structures for the 1- to 2-μm Region

R.T. Bate, J.M. Caywood, K.L. Lawley,
A.R. Reinberg and W.C. Rhines

15 June 1973

Report 08-73-30

Sponsored by
Advanced Research Projects Agency
ARPA Order No. 2182

Monitored by
U.S. Army Electronics Command
Night Vision Laboratory
Fort Belvoir, Virginia

ARPA Order No.:	2182	Project Scientist and Phone Number:	W.C. Rhines, (214) 238-5164
Program Code No.:			
Contract No.:	DAAK02-73-C-0093	Effective Date of Contract:	29 November 1972
Contractor:	Texas Instruments Incorporated Central Research Laboratories P.O. Box 5936 Dallas, Texas 75222	Contract Expiration Date:	29 November 1973
		Amount of Contract:	$152.975
		Short Title of Work:	Semiconductor-Insulator Structures for the 1- to 2-μm Region.
Principal Investigator and Phone Number:	R.T. Bate, (214) 238-3036		

This research was supported by the Advanced Research Projects Agency of the Department of Defense and was monitored by U.S. Army Electronics Command, Night Vision Laboratory, Ft. Belvoir, Virginia, under Contract No. DAAK02-73-C-0093.

Semiannual Technical Report
Semiconductor-Insulator Structures for the 1- to 2-μm Region

Contract No. DAAK02-73-C-0093

R.T. Bate, J.M. Caywood, K.L. Lawley,
A.R. Reinberg and W.C. Rhines

Sponsored by
Advanced Research Projects Agency

Prepared by
Texas Instruments Incorporated
Central Research Laboratories
P.O. Box 5936
Dallas, Texas 75222

Report Summary

The goal of this contract is to develop, fabricate, evaluate, and deliver to NVL thin-film structures consisting of semiconductors having band-gaps on the order of 0.7 eV and compatible insulators. The following requirements are also goals:

High-field tunneling transport

Semiconductor surface passivation

Semiconductor masking for diffusion and selective etching

Surface charge transport

Antireflection coatings.

Activities of the program include semiconductor material preparation (GaInAs), insulator preparation, and characterization by both electrical and nonelectrical techniques of semiconductor-insulator structures.

The primary semiconductor vehicles for this study have been GaSb and GaInAs, but early work was done on germanium; silicon was used as a control substrate for insulator depositions throughout the program. Present plans are to concentrate for the remainder of the program on $Ga_{0.5}$ $In_{0.5}$ As, which has a 0.7-eV band-gap, and to continue to use silicon as a control substrate.

The emphasis in insulator preparation has been on low-temperature processing, to prevent degradation of semiconductor properties. Three techniques are being explored: reactive plasma deposition (RPD) which is being used to deposit AlO_x, SiO_x, and SiN_x; liquid-phase anodization for native oxides and sulfides; and plasma anodization also for native insulators.

Electrical measurements indicate that preparation by all of these techniques can produce interfacial state densities as low as a few times 10^{12} cm^{-2} but only extreme care will reduce the pinhole density to acceptable levels in deposited insulators. Anodized insulators are essentially pinhole-free, but as-grown liquid-phase anodized insulators can exhibit large leakage currents and low breakdown voltages.

The present approach recognizes that deposition of insulators will probably result in low processing yields; the major emphasis during the remainder of the program will be on liquid-phase and plasma-anodized insulators.

TABLE OF CONTENTS

LIST OF ILLUSTRATIONS

LIST OF TABLES

SECTION I
INTRODUCTION

The goal of this contract is to develop, fabricate, evaluate, and deliver to NVL thin-film structures consisting of semiconductors having bandgaps on the order of 0.7 eV and compatible insulators. The following requirements are also goals:

High-field tunneling transport

Semiconductor surface passivation

Semiconductor masking for diffusion and selective etching

Surface charge transport

Antireflection coatings.

Activities of the program include semiconductor material preparation (GaInAs), insulator preparation, and characterization by both electrical and nonelectrical techniques of semiconductor-insulator structures.

The primary semiconductor vehicles for this study have been GaSb and GaInAs, but early work was done on germanium; silicon was used as a control substrate for insulator depositions throughout the program. Present plans are to concentrate for the remainder of the program on $Ga_{0.5}\ In_{0.5}\ As$, which has a 0.7-eV band-gap, and to continue to use silicon as a control substrate.

The emphasis in insulator preparation has been on low-temperature processing, to prevent degradation of semiconductor properties. Three techniques are being explored: reactive plasma deposition (RPD) which is being used to deposit AlO_x, SiO_x, and SiN_x; liquid-phase anodization for native oxides and sulfides; and plasma anodization also for native insulators.

SECTION II

SEMICONDUCTOR PREPARATION (GaInAs)

GaInAs alloys have the important property of exhibiting optical band gaps between 0.9 and 3.6μm. The particular wavelength is controlled by the ratio of Ga to In in the ternary alloys. This point is shown in Figure 2-1, in which the optical band gaps expressed in energy and wavelength are shown as a function of the mole fraction of InAs in the ternary alloy. The energy curve at 300°K was extracted from four sources.[1,2,3,4] Data[1] at 77°K are also included. This investigation is primarily concerned with materials with 1.8-μm band-gap response. In the GaInAs material systems, this gap corresponds to the composition $Ga_{0.47}$ $In_{0.53}$ As. Several other compositions, with both higher and lower InAs contents, are being investigated. In addition to composition, both p- and n-type materials with carrier densities between 10^{16} and 10^{18} /cc are being prepared. An additional requirement is that these alloys should have smooth, structureless, strain-free surfaces for the fabrication of test structures and devices.

An alloy-source vapor-phase system was used to prepare the initial material for this program. In this system an alloy of In and Ga is exposed to HCl and the reaction products mixed with AsH_3. This mixture is passed over a GaAs substrate, oriented 2 degrees toward $<111>$ on the (100) plane, upon which an epitaxial layer of the alloy is deposited. This system shown in Figures 2-2 and 2-3, can be used for growing both p- and n-type material in all composition ranges. Typical growth conditions are given in Figure 2-2. As reported by Bailey,[5] and Minden[6] the composition of the epitaxial film is not related linearly to the composition of the alloy source. Bailey's and Minden's results are shown in Figure 2-4. Present results on growth from an alloy source agree qualitatively with these observations. Continued use of a particular alloy source results in films with increasing InAs content. This results from the difference in reactivity between Ga and In with HCl. Thus, long-term compositional predictability and stability are limited. To illustrate this point, after 70 hours of use, the composition of sequentially grown alloys increased from about 20 to 80 percent InAs or about 0.9 percent/hour. Growth rate in this reactor is about 10 μm/hour; therefore, composition grading would be about 2 percent in a 20-μm-thick film. Greater gradings are suspected to actually occur. Even though grading is a natural consequence of this process, grading from the substrate composition, i.e., GaAs, to a given alloy composition is not possible because of the fixed alloy composition. This grading capability is necessary to minimize the strain resulting from the lattice mismatch between the epitaxial alloy films and the substrate.

Despite the anticipated problem associated with the alloy source reactor, an intermediate supply of material has been prepared. Films with alloy composition ranging from 20 to 80 percent InAs have been grown. These films are normally n-type, with donor densities of 1 to 5×10^{16} /cc. Surprisingly, electron mobilities of about 3,000 to 5,000 cm^2/V-sec are observed for all compositions. This value is a factor of 40 lower than the best 80 percent InAs alloys prepared by Conrad, *et al.*[7] The mobility for good lower InAs content alloy would be expected to be 8,000 to 9,000 cm^2/V-sec. This difference is attributed to the badly strained lattice of the alloy. Compensation with unknown acceptors may also be a problem. During the program, a substantial reduction of the net donor density by a factor of 100 was accomplished by improving the quality of the reactants and modifying growth condition and the reactor design. Because this reactor system is being used on an interim basis, no further work on improving the purity of the alloys will be pursued.

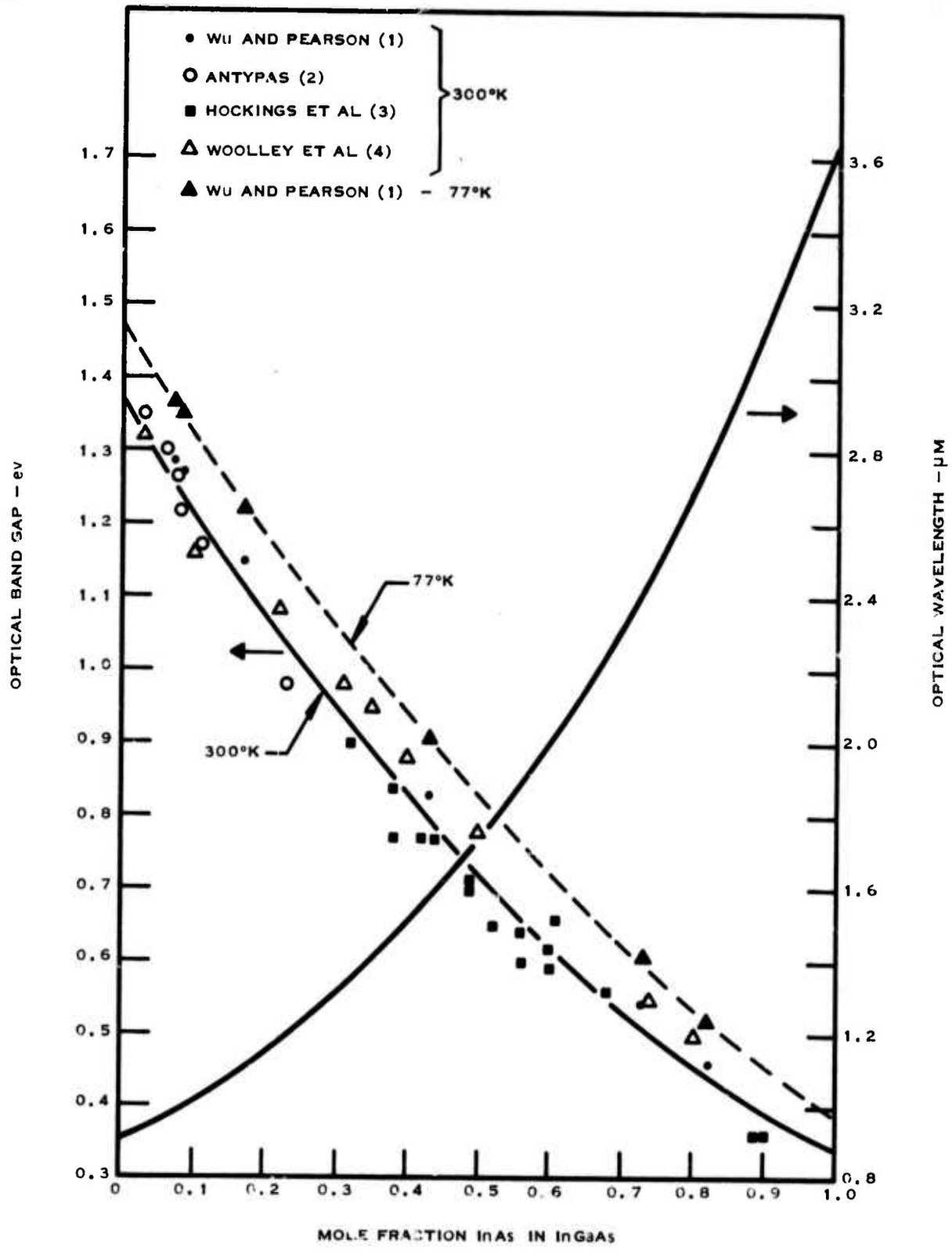

164347

Figure 2-1. Variation of the Optical Band Gap at 300°K and 77°K of the InGaAs as a Function of the InAs Content

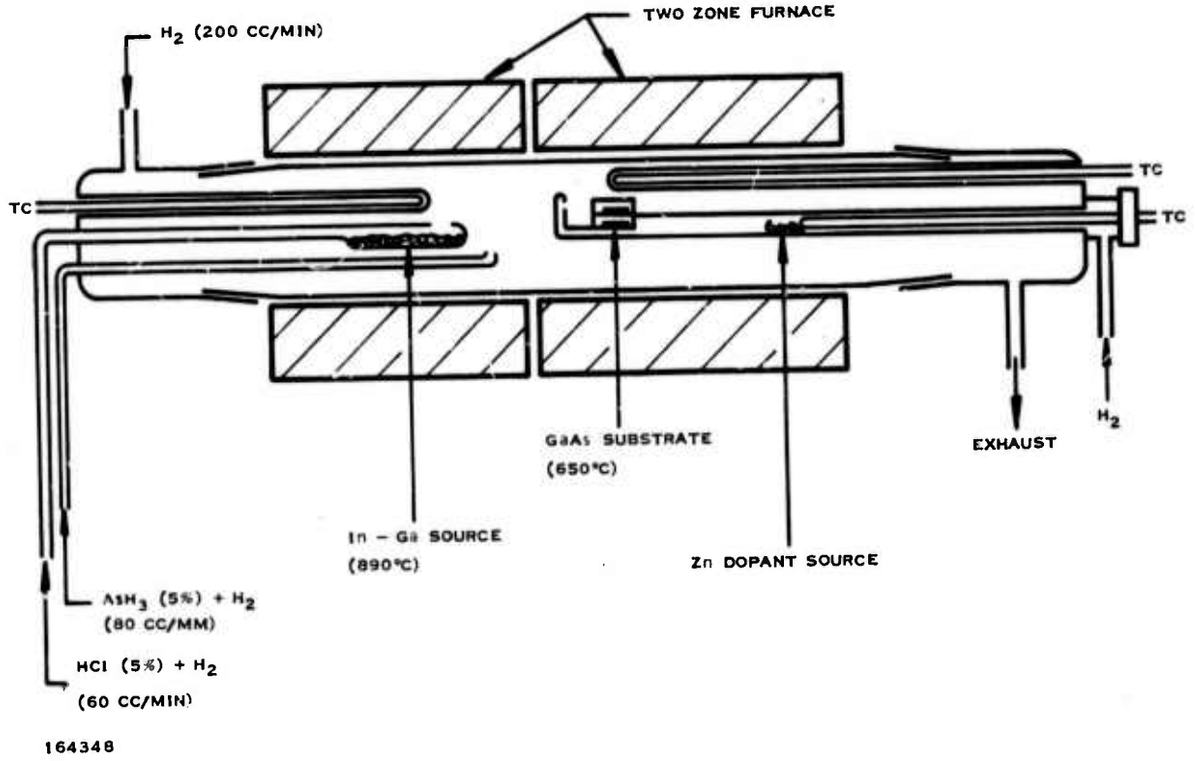

Figure 2-2. Schematic Diagram of Alloy Source GaInAs Reactor

P-type GaAs films have also been grown. Elemental zinc is being used as the source of zinc vapor which is transported into the reactor by H_2. Three runs were made under different conditions of temperature and flow of the zinc source. The only p-type sample, Film 1, had an acceptor density of 3.8×10^{17}/cc and hole mobility of 121 cm^2/V-sec. The composition was approximately 80 percent InAs. The two other runs resulted in films with the following characteristics: Film 2, n = 1.9×10^{16}, μ_e = 105 cm^2/V-sec; Film 3, n = 2.3×10^{16}/cc, μ_e = 5.400 cm^2/V-sec. Film 3 was grown with conditions identical to those which produced the p-type material on Film 1. Film 2 is obviously very closely compensated. From these preliminary observations, it appears that acceptor densities between 10^{16} and at least mid-10^{17}/cc can be achieved. Results from the analogy with other materials systems suggest this range can easily be extended to 10^{19}/cc.

Hall-effect measurements were used to characterize the electrical properties of the films. Thickness of the films were determined by standard cleaving and staining techniques. The etch used to delineate the epitaxial film-substrate interface was 1 gm KOH + 1 gm $K_3Fe(CN)_6$ in 10 mlH_2O. Visible reflectance measurements are used for the determination of the alloy composition. This method, developed by C.E. Jones.[8] has the advantage of defining the composition at the surface of the film. Correlation of reflectance with X-ray diffraction results shows the surface to be about 40 percent higher in InAs than the diffraction results would indicate.

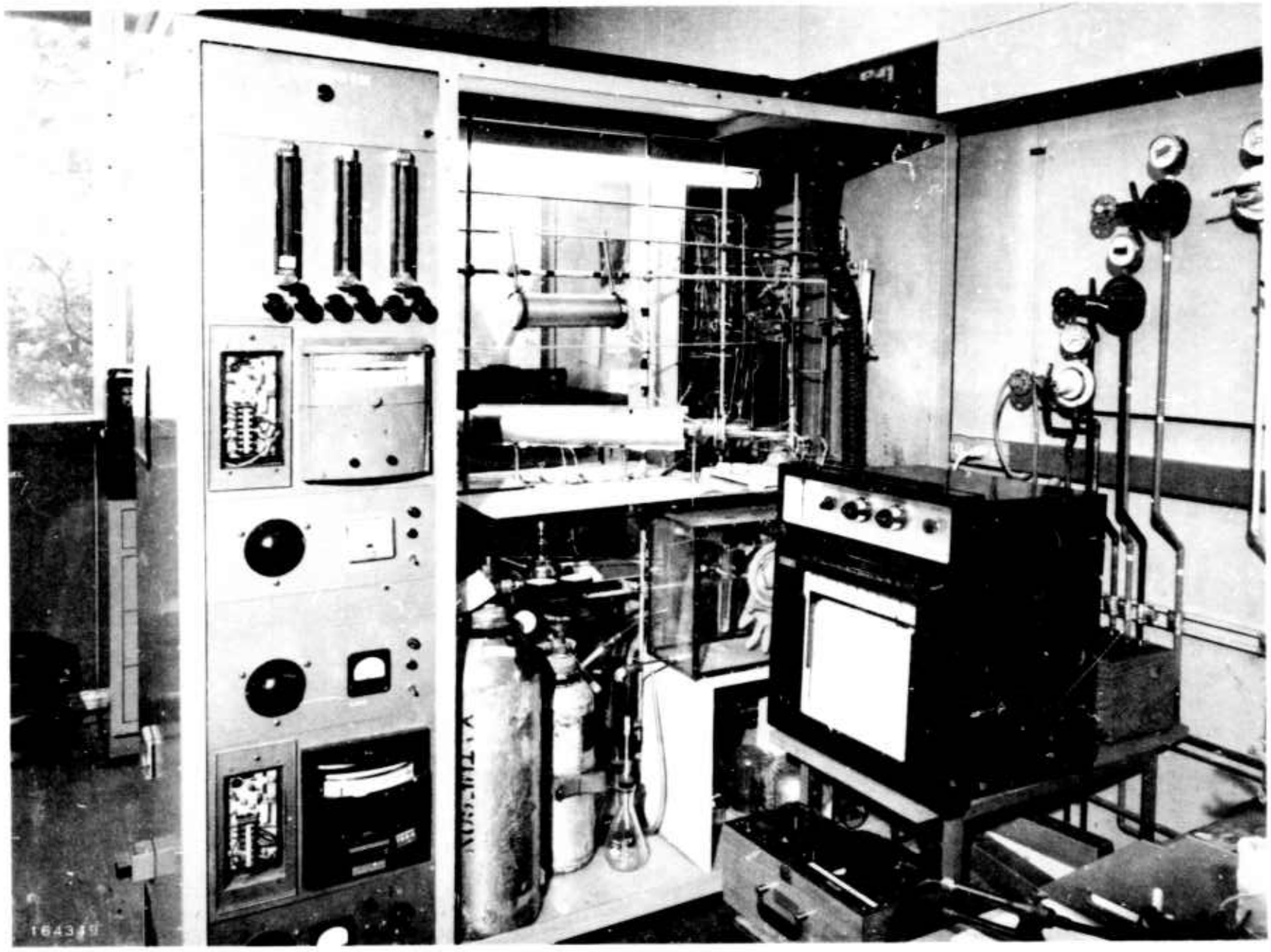

Figure 2-3. Alloy Source Epitaxial Reactor Installation

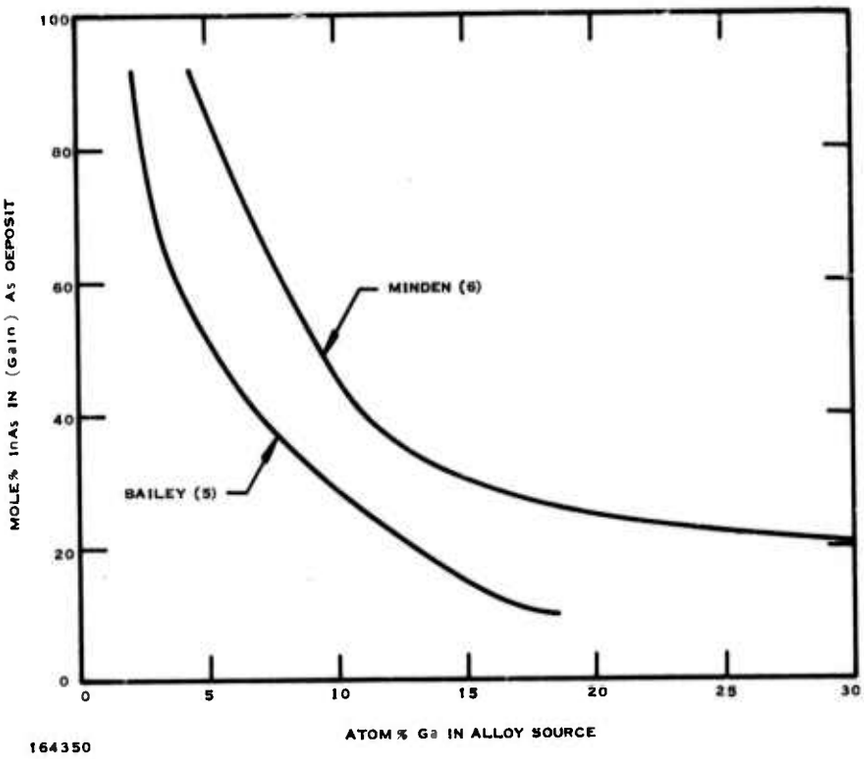

Figure 2-4. Film Composition of InGaAs Alloys as a Function of Alloy Source Composition

To improve both the properties of the alloys and the control of the growth parameters, a new dual-source reactor is being assembled. Instead of the alloy source for In and Ga, this reactor has separate inputs for In and Ga so that the In-Ga ratio can be more accurately controlled. This system will allow for grading the epitaxial film to reduce strain. The chemistry of the new system is essentially the same as that of the alloy source reactor. Arsine, HCl, and H_2 are the reactant gases with separate liquid metal sources of In and Ga. Construction of this reactor has been completed except for the installation of some temperature-monitoring equipment. Start-up is scheduled for the first week in June.

In summary, an alloy source reactor has been used to prepare GaInAs alloys with compositions ranging from 20 to 80 percent InAs. Both p- and n-type films have been grown. Major emphasis has been on n-type films with donor densities in the mid-10^{16} /cc range. Future work will be concentrated on p-type samples. Structural perfection remains the most important outstanding problem. The development of the dual-source grading reactor should minimize this difficulty. Higher mobility and better surface perfection should result from this development.

SECTION III
INSULATOR PREPARATION

A. REACTIVE PLASMA DEPOSITION

Reactive plasma deposition is a chemical vapor deposition (CVD) method of producing thin films of dielectric insulators. It differs from ordinary CVD in that all or part of the energy necessary to initiate the reaction is provided by the collisional excitation obtained in a low-pressure discharge of the reactant gases. Although plasma polymerization of organic compounds[9] is a well-known process with a long history, the process for depositing inorganic films, particularly silicon-nitrogen compounds, was first reported in 1965 by Sterling and Swann.[10]

Organosilicon films formed by an RF plasma polymerization process[11] have been found to be useful as dielectric waveguides for integrated optical devices. Interest in the inorganic films, however, has been concerned primarily with their possible uses as insulators for various types of electronic and semiconductor devices. Of most significance for this application is the fact that films may be deposited at low temperatures, precluding the need for special constraints on substrate conditions. Thus, it is possible for deposit high-quality dielectric films on materials that cannot, for one reason or another, be subjected to high temperatures. In addition, the RPD method provides a degree of flexibility in material selection not available from other low-temperature processes such as sputtering.

A simple form of reactor for the deposition of thin films, either by ordinary CVD or by RPD, consists of a horizontal tube through which the gases are allowed to flow. For some types of reactions, it is possible to stack material, such as silicon slices, so that they fit into the tube with their faces perpendicular to the tube axis. It is much more common in CVD reactors, however, to have material lie flat with the face to be coated parallel to the direction of the tube axis, which is also the direction of gas flow. This geometry also provides a simple means of obtaining uniform RF-excited glow discharges and is shown in Figure 3-1. Apparatus similar to this has been used to deposit a variety of films. The three most widely investigated materials are silicon nitride, silicon oxide, and aluminum oxide.

Silicon nitride (or, more properly, polysilazane) as deposited by RF plasma techniques is a glassy, completely amorphous material the properties of which depend on the composition of the reactant gases and the temperature of deposition. An excellent description of the nature of these glassy silicon-based compounds has been given by Phillip.[12, 13] Basically the structure of these materials is believed to consist of Si tetrahedra of the type Si-($Si_xO_yN_z$) with x, y, and z determined in a statistical manner from the concentrations of the respective species in the gas phase.

The silicon nitrides used thus far in this study have been grown from gas mixtures containing SiH_4:N_2:NH_3:Argon in various ratios. The particular ratio depends on the temperature of the deposition and the refractive index of the film that it is desired to produce. Table 3-1 is a compilation of the gas composition used to obtain a refractive index of 2.0 at temperatures ranging from 100° to 350°C. Values given are the fraction of the total gas flow for each component.

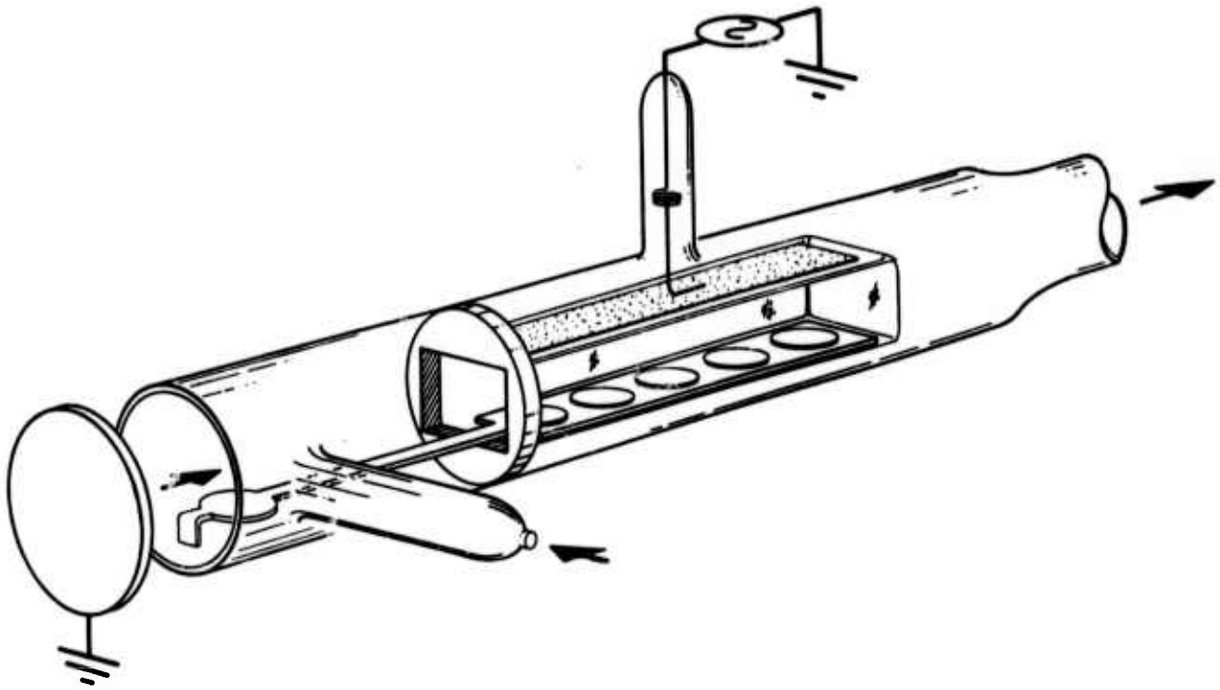

Figure 3-1. Tube Reactor w/Square Insert Tube and Gas Block

TABLE 3-1. GAS COMPOSITION TO OBTAIN REFRACTIVE INDEX OF 2.0

Temperature (°C)	SiH_4	N_2	NH_3	Ar
100	0.021	0.483	0.011	0.485
250	0.019	0.454	0.016	0.510
300	0.018	0.427	0.021	0.534
350	0.017	0.401	0.026	0.555

It is significant that the amount of ammonia needed to produce material with an index near 2.0 increases substantially as the substrate temperature used during deposition is increased from 100°C to 350°C. It may be correlated with the increase in density of the films. Figure 3-2 shows the density of the films as determined by weighing a known thickness as a function of the substrate temperature during deposition. It is well-known that the refractive index of nitrides or oxides increases as the silicon content of the film exceeds the stoichiometric concentration. The refractive index, n, also depends linearly on the density ρ, of the films according to the relation

$$\frac{n^2 - 1}{n^2 + 1} = \sum_i \frac{\rho_i B_i R_i}{W_i}$$

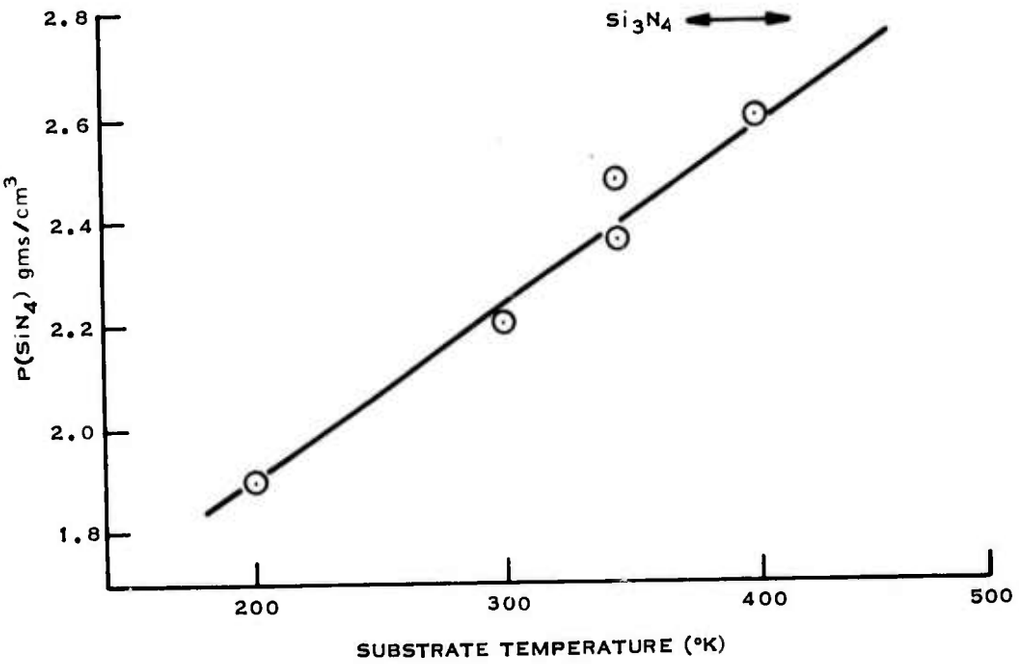

Figure 3-2. Density of Si_3N_4 Plasma-Deposited Films as a Function of Deposition Temperature

In this expression, R_i is the bond refractivity of the *ith* type of bond, B_i is the bond fraction, and W_i is the molecular weight. The summation is taken over all types of bonds present in the material. For example, for Si_3N_4, the bond refractivity, R_i refers only to the Si-N bond and has a value computed to be 1.93; B_i = 12 and $W_{Si_3N_4}$ = 140. The value of R for an Si-Si bond is considerably greater, being about 5.9. Thus, small excesses of silicon can substantially increase the refractive index. For films prepared at the lower temperature, the silicon content for fixed refractive index is expected to be greater than for films prepared at higher temperatures since the density is less. The density of the films prepared in this manner compares very favorably with that of those reported by Meyer and Scherber[14] for plasma-deposited nitrides made from silane and N_2.

Silicon oxides (polysiloxanes) have been prepared for evaluation as insulators in a manner similar to that for the nitrides but with different gases. Originally, a silane:argon-nitrous oxide:nitrogen composition was used. This system has the advantage that the structure of films is relatively insensitive to the gas composition, if the nitrous oxide concentration exceeds about 10 percent of the nitrogen concentration. An oxygen-containing gas is used (rather than pure O_2) which does not react with silane except in the region in which the glow is established. It was observed that, when the oxygen containing gas was N_2O, there was always a small homogeneous reaction that produced a fine powdery silica product. This product was detrimental to the vacuum pumps used and is also believed to produce powdery deposits that lead to pinholes. It is not known if the homogeneous (gas phase) reaction is a true small but finite reaction rate between the silane and the N_2O; if it is caused by a thermally induced decomposition of the N_2O and subsequent reaction between the SiH_4 and the resultant O_2, or if it is a result of

impurities in the N_2O which can be obtained only in medical grade. Mass spectrometer measurements failed to reveal the presence of free O_2 in the bottled gas; the major impurity was identified as argon. The Matheson Gas Data book, however, lists the principal impurity as being about 1.5-percent air which would explain the small homogeneous reactions observed.

To avoid the possible complications of the homogeneous reaction, the oxygen-bearing gas was switched to instrument grade CO_2, a 99.99-percent minimum purity. No homogeneous gas reaction has been observed with this system. Use of CO_2 is complicated by the fact that film stoichiometry, as indicated by refractive index measurements, is much more sensitive to gas concentrations. Very high CO_2:SiH_4 ratios are needed to produce films with indices near 1.46, the accepted value for silica. For these films, the ratio SiH_4:Ar:CO_2 = 0.008:0.146:0.846. It is possible with this system to produce films with widely varying amounts of silicon, going all the way from amorphous silicon to a subsilicon oxide. The structure of these films has also been discussed by Phillip.[12]

Film-density measurements have been made only for oxide films prepared at a substrate temperature of 300°C. The measured value is 2.18 gms/cm^3 which compares favorably with the accepted value of 2.21 gms/cm^3 for fused silica.

B. PLASMA ANODIZATION

Gaseous, or plasma, anodization has been used to produce many types of devices, including capacitors, Josephsen junctions, MOS transistors, tunnel barriers, and others. A recent review of the process is given by Dell'Oca, Pulfrey, and Young.[15] Two different types of anodization methods in plasmas are readily distinguished. In the first, a dc discharge is established with an appropriate potential (this may be either a cold-cathode or a hot-cathode discharge). The material to be anodized is biased positively at a different voltage with respect to the plasma to supply the anodization current. In the second method, an oxygen plasma is created by a microwave discharge and the sample is placed in the afterglow, again with an appropriate bias. Both of these techniques appear to have serious problems. In the dc technique, high voltages are necessary as is a three-electrode system. The many regions of a dc glow discharge require careful sample placement if reproducible results are to be obtained. Thus far, it appears as if a microwave-supported discharge is not capable of uniform processing over a large enough sample area to make it practical. A third method which appears not to have been reported previously is that of using an RF-supported discharge to create the plasma, with additional dc biasing to supply the anodization current. This last technique is the one that has been investigated in this program. The experimental apparatus is shown schematically in Figure 3-3. It is a simple modification of the apparatus used for plasma chemical deposition. The conducting slice holder shown in Figure 3-1 is replaced with a quartz plate on the bottom of which a thin platinum wire is strung. At several points along the quartz, holes are drilled and the platinum wire is extended to the upper surface where it serves as a contact to the back side of a slice. When placed in the inner, rectangular cross-section tube, the platinum wire is shielded from the discharge by the quartz plate. A rectangular slot is cut into the upper section of the inner rectangular cross-section tube and another quartz plate, one side of which has been coated with fired-on platinum, constitutes the other electrode. A hole in this plate supports a platinum wire, which is brought to the top of plate and makes contact with the outside world through the spring electrode.

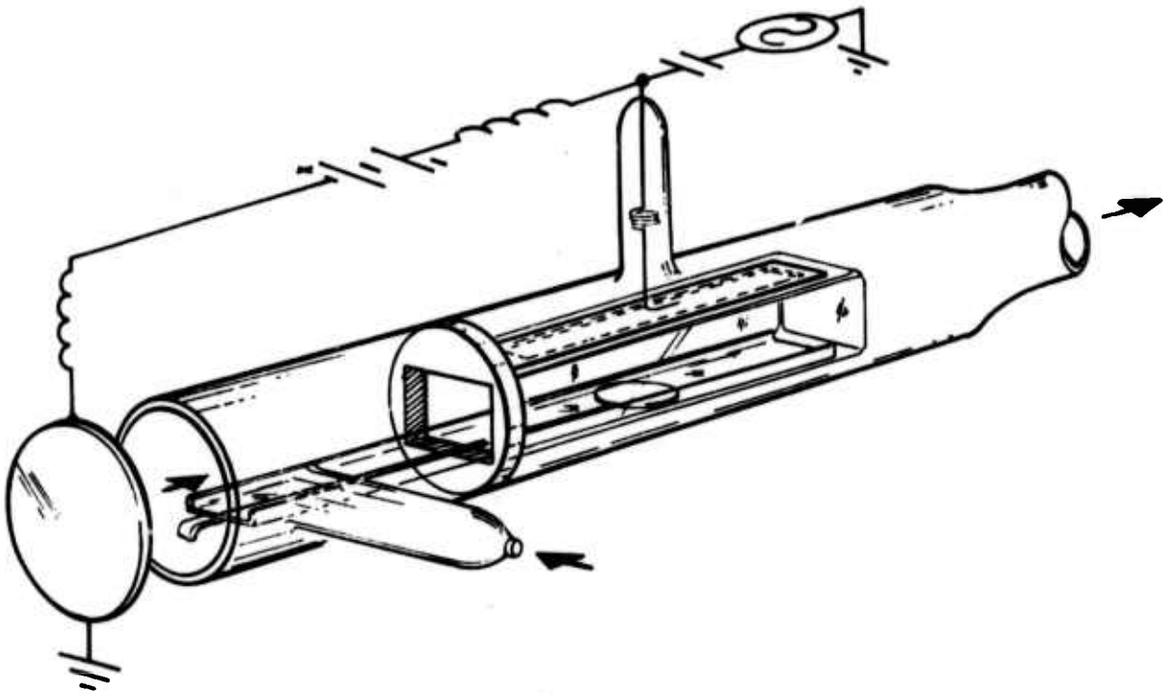

Figure 3-3. Diagram of Plasma Anodization Apparatus

This apparatus has the important property that all metal parts in contact with the plasma are made of platinum (except for the part to be anodized). The RF generator and the dc bias supply are isolated from each other by appropriate inductors and capacitors.

Thus far, this apparatus has been used for only a few exploratory runs. There has been some difficulty in monitoring the actual anodization current so that quantitative results have not yet been obtained. It has been used to anodize silicon to a thickness in excess of 500Å in 20 minutes, using a total dc bias voltage of 180 volts. All of this bias does not appear across the silicon, as the voltage drop both in the plasma and across the electrode is probably quite large. Further experiments with this apparatus are anticipated in the next period. One interesting possibility of this apparatus is that it can be used to anodize a sample and then to deposit a plasma film, as discussed in the previous subsection.

C. LIQUID PHASE ANODIZATION

1. Introduction

Anodization uses an electric field-assisted reaction of oxygen with a solid to form an insulating oxide film. Extensive reviews of the subject are available.[16,17] Anodization has been studied extensively because of its importance in corrosion as well as in the fabrication of insulator films for electrical components. The first field-effect transistor ever fabricated used an anodic oxide film on Ge,[18] but subsequent success in the growth of thermal oxides on Si made anodization unnecessary.

For growth of insulators on compound semiconducting materials, however, anodization offers some distinct advantages:

It is a low-temperature process; high-temperature processes lead to vaporization of the more volatile group V species in III-V compounds, causing surface damage and stoichiometric alterations in the semiconductor.

It offers inherently self-healing film growth. Pinholes which may develop in the insulator become points of maximum electric field and are therefore eliminated by more rapid insulator growth.

It eliminates the original semiconductor surface from the final MIS structure. This is an advantage over deposited insulators, where structural damage and contamination on the semiconductor surface lead to undesirable semiconductor-insulator interface properties.

Studies conducted during this program have used both liquids and plasma as the electrolytes for anodization. Plasma anodization offers the distinct advantage of freedom from impurity contamination, but it is a more difficult process to control than liquid anodization. Although the use of a liquid electrolyte has been reported to result in deleterious electrical effects caused by incorporation of water and OH ions in the films,[19] methods are available for "baking-out" these contaminants; some anodic films show desirable insulator characteristics even without such a process.[20]

2. Approach

Three approaches to the liquid anodization process have been attempted under this program:

1. Direct anodization of the semiconductor in an oxidizing solution.
2. Anodization of a metallic surface film and a portion of the underlying semiconductor.
3. Anodization of the semiconductor followed by plasma deposition of SiO_x on the anodic film surface.

The first anodization approach has been reported for InSb,[21] GaAs,[22] and GaP.[23] The oxides formed on InSb in aqueous KOH solutions have been successfully used for field-effect devices.[24] This type of anodization is the principal technique used in Texas Instruments program, but a modification which has not been reported previously has been used with some success. In the modification, solutions containing anions other than oxygen (principally sulfur) have been used as electrolytes. Such an approach provides a variety of insulators, other than oxides, for evaluation in MIS structures.

The second approach has not yet proved successful in Texas Instruments work and will not be discussed in this report. Very few samples were fabricated using this metal anodization technique, and a complete evaluation will require further investigation. It should be noted, however, that the approach has been successfully applied by others to silicon samples coated with aluminum.

The third approach, involving the use of a plasma-deposited overcoat for the anodic oxide, has not been reported, but is currently under investigation in this program. Although data are as

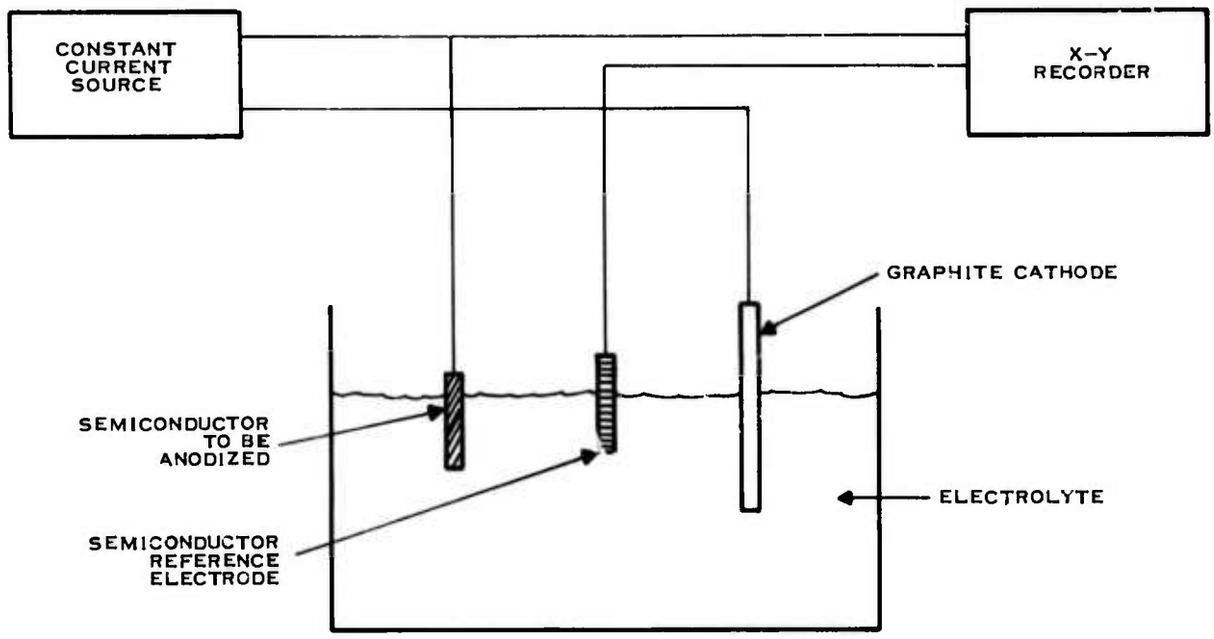

Figure 3-4. Anodization Apparatus Wired for Constant Current Operation

yet insufficient to report any promising results, the discussion portion of this section will summarize some of the reasons why this technique may be valuable.

3. Experimental Procedure

The apparatus used for anodization is shown in Figure 3-4. The reference electrode serves to counterbalance the solution potential and is made of the same semiconductor material as the anode. The apparatus can be easily altered for operation at constant current, constant voltage, or programmed ramp voltage.

Water, glycerine, and ethylene glycol have been used as electrolyte solvents. The latter two are used in cases where anodization is to be done at large voltages, exceeding the decomposition potential of water. Most anodic oxidation has been performed on GaSb, GaInAs, and Ge, using approximately 0.1 N KOH dissolved in these solvents, although other oxidizing solutions, such as NH_4OH and H_2O_2, have also been used. Attempts to form sulfide films have been made with Na_2S and sulfurated K_2CO_3 in the same solvents.

Variables that have been used to alter anodization characteristics include temperature, anodization time, current or voltage condition, solute concentration, and incident illumination.

Back sides of the semiconductor samples are normally masked during the anodization either with one of several types of photoresist or with black wax. Following anodization, the samples are rinsed in organic solvents and water, and then characterized, using optical microscopy,

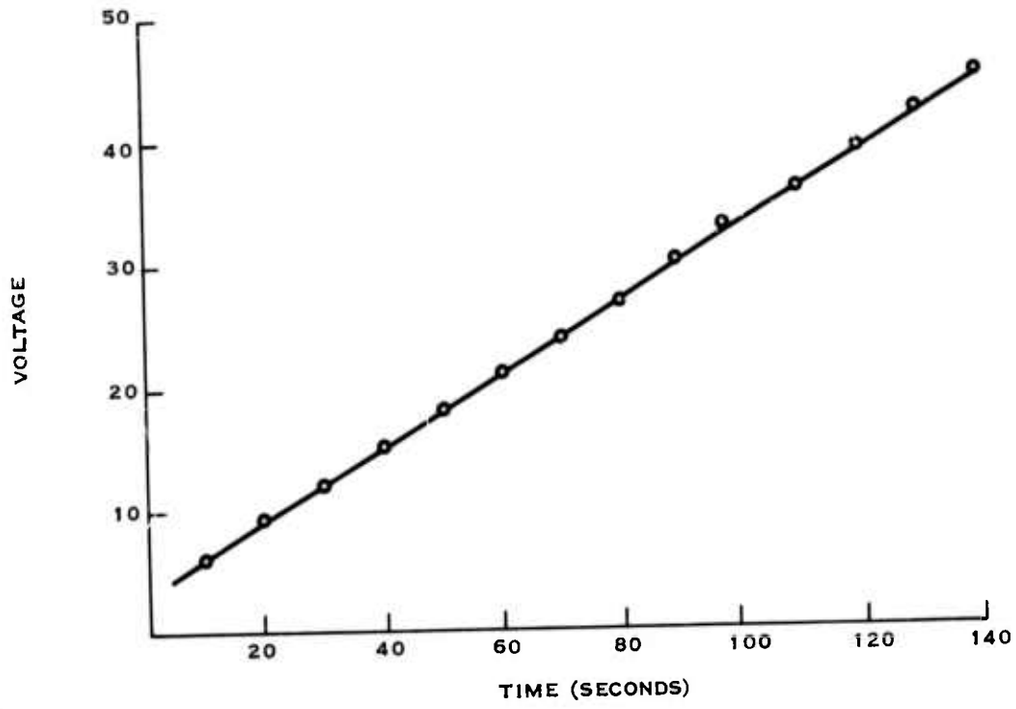

Figure 3-5. Constant Current Anodization of GaSb in 0.1 N KOH 30°C, 0.4 mA

scanning electron microscopy, and dielectric-defect detection (pinholes). Metal dots are normally deposited on the insulator surface and the electrical characterization performed.

4. Results

The most notable results on GaSb and GaInAs have been achieved using the 0.1N KOH-ethylene glycol electrolyte. For both these materials, the C-V response has been more pronounced and has shown a smaller hysteresis for the anodized films than for any of the plasma-deposited insulators. There have been two major problems however. With the GaSb, the more promising anodic films have not been reproducible. For GaInAs, the anodic film can be reproduced, but in all cases it has exhibited breakdown at voltages greater than 5 volts.

The anodic films grown on GaSb and GaInAs in sulfide solutions have, in general, been less satisfactory than have the oxides, as far as C-V characteristics are concerned. Almost all of the anodic films that were grown during this study have been shown to be pinhole-free.

A typical voltage-time curve is shown in Figure 3-5 for growth of an anodic oxide on GaSb with a constant current source at 0.4 mA/cm^2. The linear dependence has been reported for constant current anodization of InSb[25] up to 10 volts, but dissolution of the anodic film normally precludes growth at higher voltage. For this reason, the GaSb is very promising because higher dielectric breakdown strengths should be achievable.

Most of the anodic films have shown no resistance to acid attack, thus making the patterning of Al for a surface planar process very difficult. Potassium iodide and potassium ferricyanide, were used to pattern Al on some of the anodic films, but these etchants appear to degrade the electrical properties of the insulators.

5. Discussion

Although the anodic films offer some distinct advantages, including promising C-V characteristics, pinhole resistance, and ease of processing, they have some serious limitations. Among these, the low breakdown voltages and incompatibility with planar processing are the most serious. The former problem can probably be partially compensated for if a proper postgrowth annealing treatment is developed. The latter problem is more difficult to overcome. For this reason, work has recently begun using the latter two approaches, i.e., anodization through a metal overcoat, and plasma deposition over the anodic film. Potentially, either approach would capitalize upon the best points of the anodization process. The advantage of having a grown, rather than a deposited, insulator should contribute to reduced interface-state densities, as has been observed with the anodic films. In addition, the pinhole-free nature of the anodic film overcomes a major problem in the fabrication of semiconductor-insulator structures. On the other hand, the metal oxide or plasma oxide should provide the increased dielectric strength and the resistance to the etchants needed for planar processing.

SECTION IV
INSULATOR CHARACTERIZATION

A. NONELECTRICAL

1. Introduction

Development of an understanding of the semiconductor-insulator interface requires knowledge of the physical, chemical, and structural properties of both the insulator and the semiconductor materials. A complete program of nonelectrical characterization of the materials used in this study has been conducted with three objectives:

To provide supporting information useful in the interpretation of the electrical characterization measurements (thicknesses, compositions, etc.)

To serve as a monitor for process control, so as to ensure uniformity, reproducibility, and general direction in development of techniques to prepare the semiconductor-insulator structures

To provide basic knowledge concerning the relationship among physical properties of the materials and the relation of these physical properties to electrical properties of the desired MIS structures.

2. Characterization Techniques

Nonelectrical characterization for the program can be divided into the categories of physical properties, chemical composition, and structural characteristics. As anticipated, the measurements of physical properties have been emphasized during the first phase of the program because they provide support for the first two objectives and provide the most useful information for a broad survey of different materials for MIS structures. As the optimization phase of the program begins, emphasis will shift to the chemical and structural characteristics of the materials for improved understanding and control of electrical properties.

Physical properties which have been examined for the insulators include thickness, index of refraction, pinhole densities, surface morphology, and substrate cleanliness. Ellipsometry (or talystepping), optical microscopy, scanning electron microscopy, and electrophoretic pinhole detection have been used routinely to measure these properties on almost all samples fabricated in the program.

The chemical composition measurements are made to determine bulk constituents in the insulators, stoichiometric variations, and trace impurity content. Techniques used included ion-backscattering, Auger analysis, X-ray diffraction, and neutron activation analysis.

Structural characteristics are being examined primarily to determine the type of bonding in the amorphous insulators and to detect crystallinity. Infrared absorption spectra have been analyzed for the bonding studies, and prolonged X-ray exposure of insulators in a Debye-Scherrer camera has been used to look for crystallinity.

3. Nonelectrical Characterization Results

To summarize some of the results of nonelectrical measurements, four areas of concern in the program have been chosen. These examples illustrate the utility of the nonelectrical characterization methods in the solution of problems in the fabrication of MIS structures and reveal some of the basic material properties that have been observed.

a. Cleaning Procedures

It was apparent very early in the study that substrate surface cleanliness is the most critical factor in the preparation of plasma-deposited insulators with suitable electrical properties and low pinhole densities. It was therefore necessary to develop specific cleaning and etching procedures for each substrate used. Characterization for this purpose included optical microscope examination of substrates (particularly with dark field and interference contrast), scanning electron microscopy, and Auger surface contamination analysis.

Silicon slices were the standard of comparison because proprietary cleaning procedures developed for integrated circuit manufacturing can be used with some reliability. Figure 4-1 is a scanning electron microscope (SEM) photograph of particulate contamination found on Si slices that had been thoroughly cleaned and then stored in plastic boxes for 2 weeks. The largest particles are about 3,000 Å in diameter. Contamination of this type was eliminated by storing all types of substrates in airtight, polypropylene boxes immediately after cleaning. In addition, cleaning was performed immediately before insulator deposition, whenever possible. Further reductions in particulate contamination were achieved when processing for the program was moved to a cleanroom facility.

Gallium antimonide presented particular problems because of the tendency for surface oxide to form during solvent rinses and because the standard III-V chemical etchants cause pitting of the surface. Clean, etched surfaces were obtained in this case by anodically oxidizing the surface and then removing the oxide with 5-percent hydrofluoric acid. It was necessary to use multiply filtered, deionized water as a final rinse, followed by drying with filtered nitrogen to prevent surface film formation.

Studies of Ge surfaces with both optical and scanning electron microscopy revealed a problem not encountered with other substrates. Figure 4-2 shows SEM photographs of polished Ge samples before and after a 30-percent hydrogen peroxide etch. The original polishing technique used on these substrates left residual subsurface damage that was not apparent upon examination before etching. This surface characterization motivated implementation of improved abrasive and chemical-mechanical polishing techniques, followed by etching and careful inspection. Currently, CP4 ($HF:CH_3COOH:HNO_3$:: 1:2:1) is providing the best etching results (see Table 4-1).

Finally, insulators deposited on some of the GaInAs epitaxial layers that were produced in the early stages of the study showed excessively high pinhole densities. Surface cleaning was not the problem in this case, as is revealed by the SEM photographs in Figure 4-3. Despite the very satisfactory HF cleaning procedure, coverage of the rough surface topography seen in Figure 4-3a was impossible. This problem was resolved quickly, as surface topographies became typified by Figure 4-3b, but SEM examination is still being used for quality control purposes on the epitaxial layers.

Figure 4-1. Particulate Contamination of a Si Slice after Storage for 2 Weeks in a Plastic Box (SEM Photograph: 20,000X)

b. *Effects of CO_2 on the Structure of Plasma SiO_x Films*

During the program, it became necessary to change from N_2O to CO_2 as the oxygen source during plasma deposition of SiO_x. Although most physical properties of the films did not change, there was some concern that they would be structurally different, particularly with respect to the possible presence of Si-C bonding. Infrared absorption measurements were used to investigate this possibility. No Si-C bonding could be detected, although minor concentrations of CO_2 were present, similar to the quantities found in films sputtered in a CO_2 ambient.[26] Since that time, no changes in electrical properties or other physical properties have been detected.

c. *Pinhole Densities*

One of the principal goals for the insulator growth effort is to reduce pinhole

A. BEFORE 30-PERCENT H_2O_2 ETCH

B. AFTER 30-PERCENT H_2O_2 ETCH

164359

Figure 4-2. Polished Ge Samples Before and After 30-Percent Hydrogen Peroxide Etch (SEM Photographs, 2,500X)

TABLE 4-1. CLEANING AND ETCHING PROCEDURES FOUND MOST SATISFACTORY FOR SUBSTRATES

Semiconductor	Etchant	Cleaning Procedure
GaSb	Anodic oxidation followed by 5-percent HF	Organic solvents plus deionized water
Ge	CP4 at 0°C	Organic solvents plus deionized water
GaInAs epilaxy	5-percent HF	Organic solvents plus deionized water

densities to a negligible level. To do this, a quick but accurate characterization method must be used to determine pinhole densities. Attempts were made to use chemical etchants to attack the substrates at pinhole sites, followed by removal of the insulator film and microscopic pit count on substrate. This technique is both destructive to the samples and time consuming. Scanning electron microscope examination of insulator surfaces is an improvement, but it is not a very satisfactory method for routine quality control. The best technique for the purpose has used the "Navionic Dielectric Defect Detector." The apparatus consists of a gold-plated dish filled with methanol, to which the semiconductor slice makes contact. A copper ring is used as the anode and is placed 0.76 mm above the insulator surface. The semiconductor serves as the cathode of an electrophoretic cell, so that when a potential of about 1 volt is applied, preferential conduction occurs at any pinholes in the insulator, and gas bubbles evolve at these points. A microscope with calibrated grid is used to provide a count of pinholes per unit area. Translation controls are available so that an entire sample surface may be examined. Theoretically, pinholes as small as 0.1 μm should be detectable with such a system.

All semiconductor-insulator structures are now routinely examined using the Dielectric Defect Detector. Samples that show excessive pinhole densities (>20/cm^2) are usually characterized further in the SEM to determine the nature of the pinholes. By operating the device at about +2 V, some decoration with copper from the anode can occur, and this decoration, though destructive for the sample, provides a permanent pattern for subsequent microscopy. When very high currents are used (greater than 8 mA), pitting of the silicon substrates has been found to occur at pinholes, as shown in Figure 4-4. The pits exhibit the symmetry of the silicon substrate, in this case (100).

Average pinhole density counts for all samples are shown in Table 4-2. Samples from the same plasma-deposition run tend to have similar pinhole densities, but there is significant variation between runs. Anodized films have shown consistently lower pinhole densities, presumably as a result of the "self-healing" effect of this growth process.

TABLE 4-2. AVERAGE PINHOLE DENSITY COUNTS FOR VARIOUS SAMPLES

Insulator	Thickness	Pinhole Density (number/cm^2)
AlO_X	~1,000 A	30
SiO_X	~1,000 A	41
SiN_X	~1,000 A	43
Liquid-anodized	~500 A	<1
Plasma-anodized	~2,000 A	<5

A. ONE OF THE FIRST OF THE SAMPLES PRODUCED FOR THIS STUDY

B. SAMPLE GROWN 1 MONTH LATER

164360

Figure 4-3. GaInAs Surface Topography (SEM Photographs)

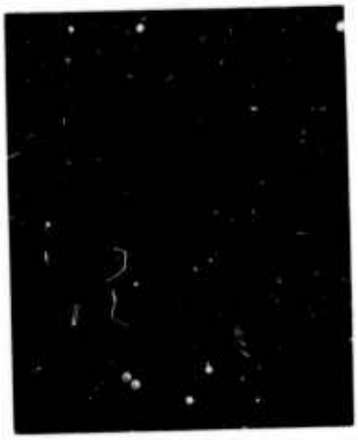

A. OPTICAL MICROSCOPE PHOTOGRAPH, DARKFIELD, 400X

B. SEM PHOTOGRAPH, 24,000X

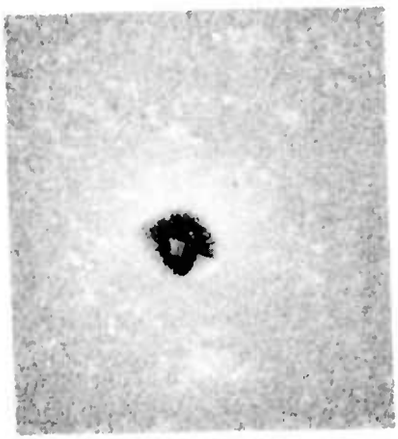

C. SEM PHOTOGRAPH, 8,000X

164361

Figure 4-4. Pitting of a Silicon Substrate at Pinholes in a 1,000-Å Al_2O_x Film

d. Impurities in Plasma-Deposited Films

Trace impurity contamination in the plasma-deposited insulators can greatly alter the dielectric properties, particularly if the contaminants are mobile ions. Neutron activation analysis provides the most sensitive characterization technique for this purpose and was used to detect impurities in the plasma SiO_x and SiN_x.

After a standard cleaning, six 2-inch slices of phosphorus-doped silicon were used as substrates for the deposition of 2.3 μm of plasma SiO_x. Six more were used for 2.6 μm of SiN_x and two were used as control samples without deposited films. Densities of these films were found to be 2.18 gm/cm^3 for the SiO_x and 2.2 gm/cm^3 for the SiN_x. All 14 slices were irradiated for 14.0 hours in a flux of 1.5×10^{13} n/cm^3/s. The results are summarized in Table 4-3.

TABLE 4-3. NEUTRON ACTIVATION ANALYSIS IMPURITY CONCENTRATIONS

	Na	Cu	As	Sb	Au	Br	Ga
Units (atoms/cm^3)	10^{15}	10^{15}	10^{14}	10^{14}	10^{12}	10^{14}	10^{14}
Detection Limits	0.1	0.3	0.05	0.05	1	0.1	0.4
SiN_x							
Mean	13.7	3.6	0.28	0.95	<1	1.3	<0.4
Standard Deviation	3.9	2.4	0.12	0.46	–	0.4	–
Probable Error (68 percent)	2.6	1.6	0.08	0.31	–	0.3	–
SiO_x							
Mean	26.5	28.8	0.80	0.14	<1	2.8	<0.4
Standard Deviation	7.1	16.9	0.18	0.09	–	0.7	–
Probable Error (68 percent)	4.8	11.4	0.12	0.06	–	0.5	–
Control Samples							
Mean	4.3	3.0	1.8	6.6	1.0	1.0	<0.4
Standard Deviation	4.7	1.3	2.2	9.8	0.4	0.9	–
Probable Error (68 percent)	3.2	0.9	1.5	6.1	0.3	0.6	–

The SiO_x films showed a definite increase in Na and Cu contamination over those of SiN_x. One possible explanation was a brass valve on the CO_2 tank that is used as a source of oxygen for the SiO_x films. Since all other valves are stainless steel, the SiN_x films would be expected to contain less Cu than the SiO_x. A stainless steel valve was substituted for the brass one in an attempt to eliminate this problem. It is also possible that the SiO_x films are more easily contaminated during subsequent handling, accounting for the increased Na contamination. This explanation has been suggested before and was attributed to the lower density of plasma SiO_x films but, in this case, the SiO_x films show densities comparable to those of the SiN_x. Thermal oxide on silicon normally contains about one-third the Na concentration observed in these plasma-deposited samples.

The other contaminants reported in Table 4-3 are of interest primarily because of potential effects of diffusion from the deposited films into semiconductors. The results indicate that no problems will be encountered from this in Texas Instruments because the total impurity content

in a 1,000-Å-thick film would provide insignificant amounts of these elements when diluted by diffusion into the bulk semiconductor.

4. Backscattering Analysis

a. Introduction to the Technique

Over the last several years, backscattering analysis has been applied to a large variety of problems such as chemical analysis of lunar soils, location and concentration of ion-implanted species in semiconductors, absorption of ink by paper, and compound formation at metal-semiconductor interfaces.[27, 28, 29, 30] Figure 4-5 shows schematically a typical apparatus for backscattering analysis. A mono-energetic, collimated beam of MeV He ions, produced by the accelerator, impinges on the target. A few of these He ions scatter back into the detector, typically an Si surface barrier device. The detector and amplifier produce voltage pulses with amplitude proportional to the energies of the particles striking the detector. These pulses are sorted according to amplitude and stored by the multichannel analyzer to produce a spectrum which displays the number of He particles in a given energy interval (channel) versus their energy.

The important points of the technique for the present application are that (1) the energies of an ion immediately before and immediately after backscattering from an atom are related by a simple constant, k^2, which depends only on the mass of the projectile, M_1, the mass of the target atom, M_2, and the scattering angle, θ; and (2) that MeV ions penetrating a solid have a very low probability of backscattering but rather lose energy at a roughly linear rate over a distance of ~1 μm. (These points are discussed in some detail in reference 31).

The implications of these two statements for the present discussion are shown in Figure 4-6. As can be seen in Figure 4-6a, if He ions are scattered from an atomically thin target consisting of a mixture of Al and Ge, two characteristic lines in the spectrum are observed, with the line produced by the heavier atom, Ge, lying at higher energy than that produced by the lighter atom, Al.

In Figure 4-6b, the spectrum from an Al layer of a few thousand angstrom units thick is shown. This spectrum begins at the location of the line from the thin layer (this location is often referred to as the Al "edge") and extends to lower energies by an amount ΔE because ions that

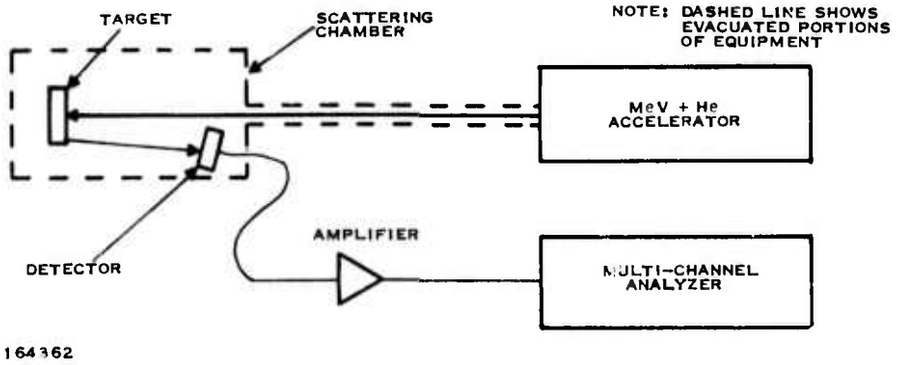

Figure 4-5. Schematic Diagram of Typical Backscattering Analysis Equipment

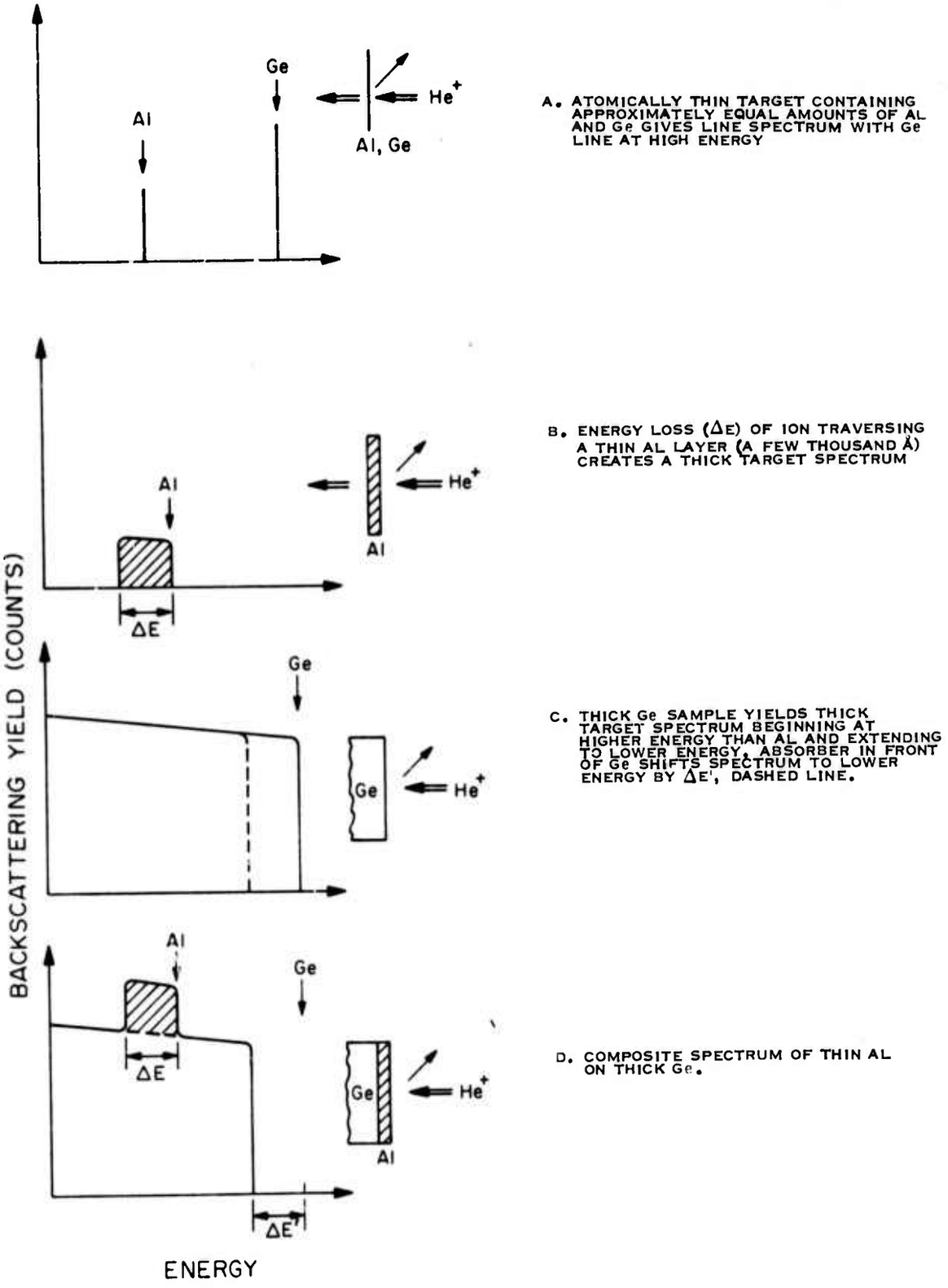

Figure 4-6. Schematic Diagrams of Various Targets and Their Resultant Backscattering Spectra

scatter from atoms within the film lose energy going into and coming out of the film and so appear at lower energies. Thus, there is an approximately linear relation between energy below the edge and depth beneath the surface. Following analogous arguments, the spectrum for a thick Ge target would begin at the Ge edge and extend to lower energies (Figure 4-6c). If a thin layer of material were placed just in front of the Ge target, the Ge spectrum would be shifted to lower energy by an amount $\Delta E'$, as shown by the dashed line in Figure 4-6c, because of the energy lost by the He ions in their traversals of the overlying layer. An Al layer deposited on a Ge target would cause just such an energy shift while the signal from this Al layer would appear superimposed on the signal from the Ge target, producing the composite spectrum shown in Figure 4-6d.

By applying these principles, one can understand the backscattering spectrum of AlO_x on a Si substrate which appears in Figure 4-7a. Here, the Si spectrum has been shifted to lower energy by the energy losses the ions scattering from the Si undergo while passing twice through the AlO_x layer. Because of the relatively low atomic mass of oxygen, the portion of the spectrum arising from ion scattering from the oxygen atoms is superimposed upon the Si background, appearing as a bump between ~0.52 MeV and ~0.74 MeV. However, since the atomic mass of Al is only slightly less than that of Si, the portion of the spectrum caused by ions scattering from Al appears only partially superimposed on the Si background, producing a peak in the vicinity of 0.92 MeV where the superposition appears. The portions of the spectrum arising from scattering from various types of atoms can be separated, as can be seen in Figure 4-7b where the Si background has been separated from the peaks arising from scattering of ions by the deposited films.

b. Experiment and Analysis

Aluminum oxide was deposited upon freshly cleaned Si wafers in an RF plasma reactor. The source and gases were trimethyl aluminum (TMA) and nitrous oxide. A number of depositions were made, differing only in the ratio of TMA/N_2O and the substrate temperature.

Backscattering analyses were made with the 3-MeV Van de Graaff accelerator of the Kellogg Laboratory of the California Institute of Technology. Typical analyzing beams had energies of 2.0 MeV and intensities of 100 nA. During a typical analysis, 120 μC was distributed uniformly over an area 1.3 mm by 1.3 mm. The energy analysis system had a resolution of ~15 keV leading to a depth resolution of ~300 Å for the materials under investigation.

The Si background spectrum was fit to a third-order polynomial in the energy regions where there is no contribution from the deposited film. The resulting polynomial approximation to the Si spectrum was subtracted from the measured spectrum. This polynomial approximation and the residue after subtraction are shown in Figure 4-8b. The rounded leading edge of the polynomial approximation arises from the finite energy resolution of the detection system, an effect which was folded into the approximation. That the approximation used for the Si background is a good one can be seen from the shape of the remainder of the experimental spectrum after subtraction.

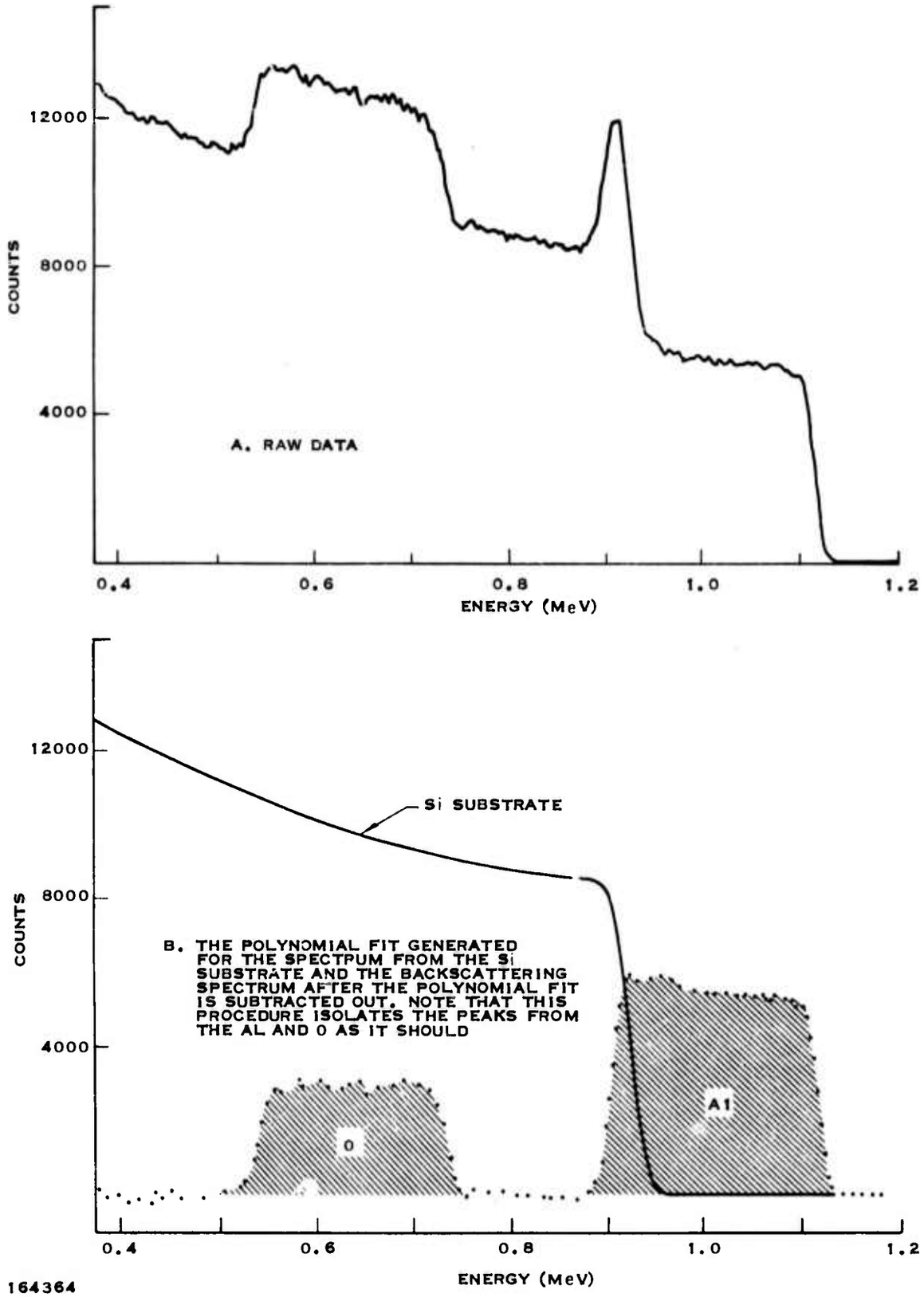

Figure 4-7. Backscattering Data from a Sample of AlO_x on a Si Substrate

$$\frac{[Al]}{[O]} = R \frac{\left.\frac{d\sigma}{d\Omega}\right|_{Al}}{\left.\frac{d\sigma}{d\Omega}\right|_{O}}$$

where R is the ratio of the total number of counts in the oxygen peak to the total number of counts in the Al peak.[31] It is known that

$$\frac{d\sigma}{d\Omega} = 1.296 \left(\frac{Z_1 Z_2}{E}\right)^2 \left[\csc^4 \frac{\theta_L}{2} - 2\left(\frac{M_1}{M_2}\right)^2 + O\left(\frac{M_1}{M_2}\right)^4\right]$$

where Z_1 and Z_2 are the atomic numbers of the projectile and target atoms, respectively, M_1 and M_2 are the atomic masses of the projectile and target atoms, respectively, and θ_L is the scattering angle in the laboratory coordinate system.[32] This leads to

$$\frac{[Al]}{[O]} = 0.3471\ R$$

c. Results

The stoichiometric ratios of the deposited layers calculated from the backscattering analyses are given in Table 4-4 as a function of temperature and gas ratio. The accuracy of the stoichiometric ratios is 1 percent. The measured indices of refraction are also given. Note that the refractive index increases monotonically with increased value of the ratio [Al]/[O]. Note also that stoichiometric ratios cluster closely about the value 0.667 expected for aluminum oxide.

TABLE 4-4. STOICHIOMETRIC RATIOS OF THE DEPOSITED LAYER CALCULATED FROM BACKSCATTERING ANALYSES

TMA/N_2O / Temperature	1/10	1/20	1/40	1/80
560°C			[Al]/[O] = 0.739 n = 1.703	
400°C	[Al]/[O] = 0.675 n = 1.643	[Al]/[O] = 0.657 n = 1.593	[Al]/[O] = 0.691 n = 1.678	
290°C			[Al]/[O] = 0.633 n = 1.526	

B. ELECTRICAL

1. General Principles

Electrical characterization has been done chiefly by capacitance-voltage (C-V) and current-voltage (I-V) measurements on metal-insulator-semiconductor (MIS) capacitors. When the semiconductor is accumulated, the capacitance measured is that of only the insulator layer,

$$C_I = \frac{AK_I \epsilon_o}{X_I} \tag{4-1}$$

where A is the area of the metal contact, K_I is the dielectric constant of the insulator, and X_I is the insulator thickness. If the semiconductor is in inversion, the measured capacitance is the series combination of the insulator and the semiconductor depletion layer,

$$C_M = \frac{C_I C_S}{C_I + C_S} \tag{4-2}$$

The semiconductor capacitance is described by

$$C_S = \frac{AK_I \epsilon_o}{X_d} \tag{4-3}$$

where the depletion layer thickness for an inverted layer is

$$X_d = 2\sqrt{\frac{K_S \epsilon_o \phi_F}{q N_D}} \tag{4-4}$$

where K_S is the dielectric constant of the semiconductor, N_D is the net ionized dopant density and ϕ_F is the potential difference between the Fermi level and the intrinsic Fermi level. Finally,

$$\phi_F = \frac{kT}{q} \ln\left(\frac{N_D}{n_i}\right) \tag{4-5}$$

if the semiconductor is not degenerate (the case of interest).

If the capacities are measured with the semiconductor both in depletion and in accumulation, Equations (4-2) through (4-5) can be solved iteratively for N_D and ϕ_F. That is, ϕ_F can be guessed and the guess used in Equations (4-2) through (4-4) to calculate N_D which can then be substituted into Equation (4-5) to solve for ϕ_F. The new value of ϕ_F can then be used to calculate N_D. Since ϕ_F depends on N_D only logarithmically, this procedure rapidly converges to yield values for ϕ_F and N_D.

Under this program, a computer program has been developed which, when given C_M, C_I, and X_I, computes K_I and N_D. This value for N_D is then compared with the value measured before the insulator was deposited to check that inversion and accumulation of the semiconductor surface were indeed obtained.

As the semiconductor surface is driven from accumulation to inversion by a bias voltage on the gate metal, there is a point at which the bands in the semiconductor are flat (i.e., bent into neither accumulation nor inversion). The bias voltage at which this occurs is of great significance for both scientific and practical reasons.

It is known that the flat-band voltage,

$$V_{FB} = \Phi_{MS} - \frac{Q_{SS}}{C_o} - \frac{1}{C_o} \int_o^{X_o} \frac{X}{X_I} \rho(X)\, d(X)$$

where Φ_{MS} is the difference in metal-semiconductor work functions, Q_{SS} is the sheet charge at the semiconductor-insulator interface, C_o is the insulator capacity, and ρ is the insulator charge distribution.[33] Since Φ_{MS} is usually known, V_{FB} is a measure of Q_{SS} and ρ. Thus, V_{FB} gives information concerning the insulator and its interface with the semiconductor.

Practically speaking, one would like to operate a CCD at modest voltages. This requires V_{FB} to be small. From this point of view, measuring V_{FB} is monitoring an important device parameter. Moreover, from the device standpoint, one requires that V_{FB} be constant under repeated voltage cycling. This property can also be checked.

A final concern is the surface-state density. Surface states cause both charge transfer inefficiency and noise in CCDs,[34,35] as well as providing a mechanism for minority carrier recombination. If the density is sufficiently high, surface states may even pin the surface potential so that the bands cannot be bent. As the surface-state density increases, the C-V curve may develop kinks or become distorted from that which one would calculate, neglecting surface states.[36] Thus, a quick examination of the C-V curve gives a qualitative measure of surface-state density and distribution, although it is difficult to extract accurate quantitative information from this measurement. Some of the difficulties involved in this determination are discussed below.

Initially there was a great deal of variation in the C-V characteristics of Texas Instruments MIS structures. In a number of cases, the surface-state density was so high that it proved to be impossible to bend the bands with the bias voltages that were available (±15 V). In these cases, the measured capacitance was independent of applied bias. Greater care in device preparation improved the reproducibility, and band bending was eventually achieved on all of the semiconductors used in performance of this contract.

Figure 4-8 shows a C-V curve typical of the better MIS structures Texas Instruments has made on GaSb. Note that the minimum value of $C/C_o = 0.93$. The anodized insulator on this sample was ~560 Å thick and had a relative dielectric constant of 5.6. This implies that $N_D \cong 3 \times 10^{17}/cm^3$, a value in excellent agreement with the value $2 \times 10^{17}/cm^3$ derived from Hall-effect measurements.

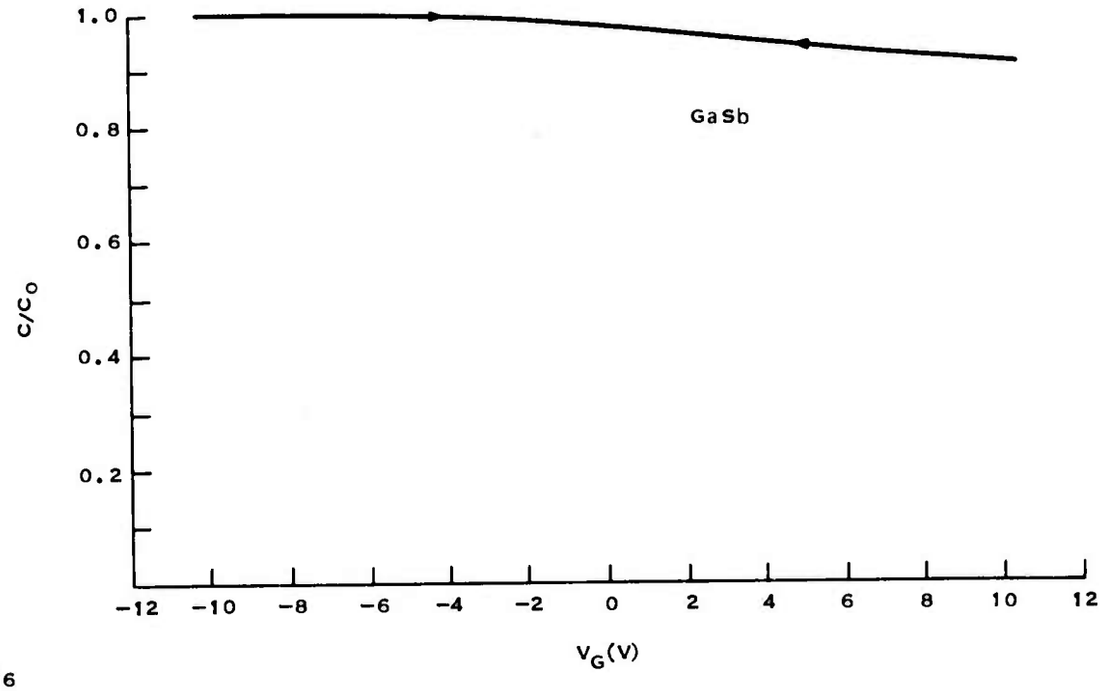

164366

Figure 4-8. Capacitance-Voltage Curve Taken on an MIS Sample (560 A of Anodized Insulator on GaSb Doped to 2 X 10^{17})

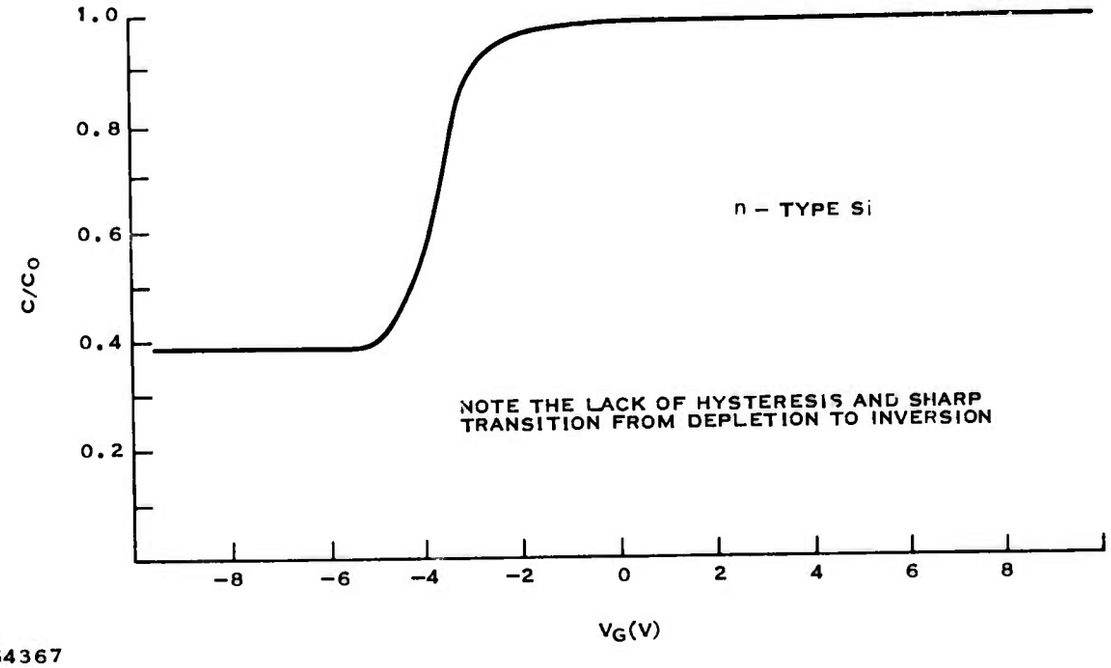

164367

Figure 4-9. Capacitance-Voltage Curve Taken on Thermally Oxidized (110) Si

More information concerning this sample can be gained from comparing Figure 4-8 to Figure 4-9 which has an almost ideal C-V characteristic. The measurement shown in Figure 4-9 was taken on a structure consisting of an n-type Si wafer which had been thermally oxidized, annealed, and then had Cr/Au deposited on it. Compare the steep slope of the C-V curve in Figure 4-9 to the gradual change in Figure 4-8 as the surface is driven from accumulation to inversion. This indicates that the GaSb/insulator interface has about 5×10^{12} /cm^2 interface states distributed fairly uniformly across the bandgap. This corresponds to a density of $\sim 8 \times 10^{12}$ /cm^2-eV. A surface-state concentration of 5×10^{12} /cm^2 is a great improvement over the value of $\sim 10^{15}$ /cm^2 expected on a freshly cleaved surface, but considerable improvement would still be required to reach the level of $\sim 5 \times 10^{10}$ /cm^2 required for a good surface-channel CCD.

Shown in Figure 4-10 is a C-V curve typical of those measured on Texas Instruments better anodized GaInAs samples. Note that the slope in the transition region between accumulation and inversion is much steeper than in Figure 4-8, indicating a smaller surface-state density. It is this improvement in surface-state density which necessitates the improvement in instrumentation for quantitative analysis as is discussed in Subsections IV.B.3 and IV.B.4. The origin of the hysteresis exhibited in Figure 4-11 is a subject of continuing investigation.

A C-V curve for RPD SiO_x on p-type Ge is shown in Figure 4-11. This curve is typical of those achieved on a large number of samples. With the exception of the hysteresis, this curve is in good agreement with what would be calculated theoretically for such a sample.

As was mentioned at the beginning of this section, current-voltage measurements were used as a means of evaluating the quality of the insulators under investigation. RPD Al_2O_3 consistently exhibited the highest values of resistivity with values in the range of 10^{16} Ω-cm typical for fields of $\sim 10^6$ V/cm. Values of 10^{14} Ω-cm were typical for RPD SiO_x at similar fields. The anodized layers are a more difficult matter. Typical values of the resistivity were 10^{10} Ω-cm at 10^6 V/cm for these layers, but occasionally resistivities as high as 10^{14} Ω-cm were measured. Since dielectric layers with resistivity greater than 10^{10} Ω-cm are needed for CCDs, effort will be expended toward increasing the resistance of the anodized layers.

2. Charge Contained in Radio-Frequency Plasma-Deposited (RPD) Insulators

The fixed charge in the insulator of an MIS structure has a profound effect on the flat-band voltage of that structure. Since RPD insulators are deposited in an environment containing large quantities of charged species, one might suspect that these insulators would incorporate copious quantities of these charge species during deposition with large resultant flat-band voltages.

It was decided that, to unambiguously determine the fixed charge in an RPD insulator, the effects of charge arising from the deposition process must be separable from those arising from an unpassivated semiconductor interface.[33] The coordinate system zero is located at the RPD insulator surface and structure extends in the positive direction. The quantities C_o and C_{RPD} are the unit capacities of the thermal oxide layer and RPD insulator layer, respectively, and are given by

$$C_o = \frac{K_o \epsilon_o}{X_o - X_I} \text{ and } C_{RPD} = \frac{K_{RPD}\ \epsilon_o}{X_I} \tag{4-6}$$

where X_o is the location of the semiconductor/thermal oxide interface.

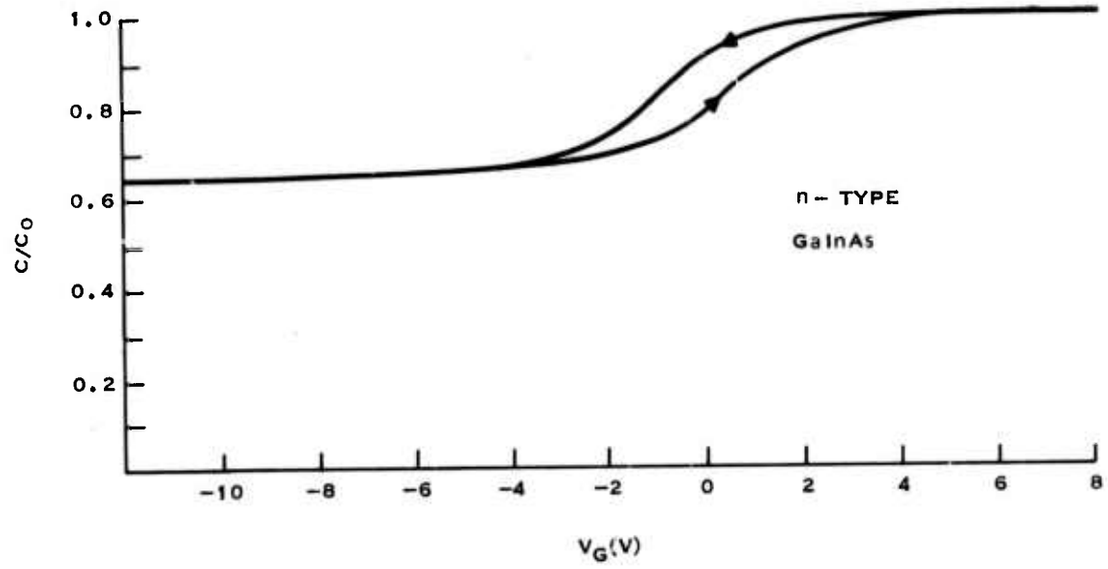

164368

Figure 4-10. Capacitance-Voltage Curve Measured on a Structure of 700 A of Anodized Insulator on $Ga_{1-x}In_xAs$

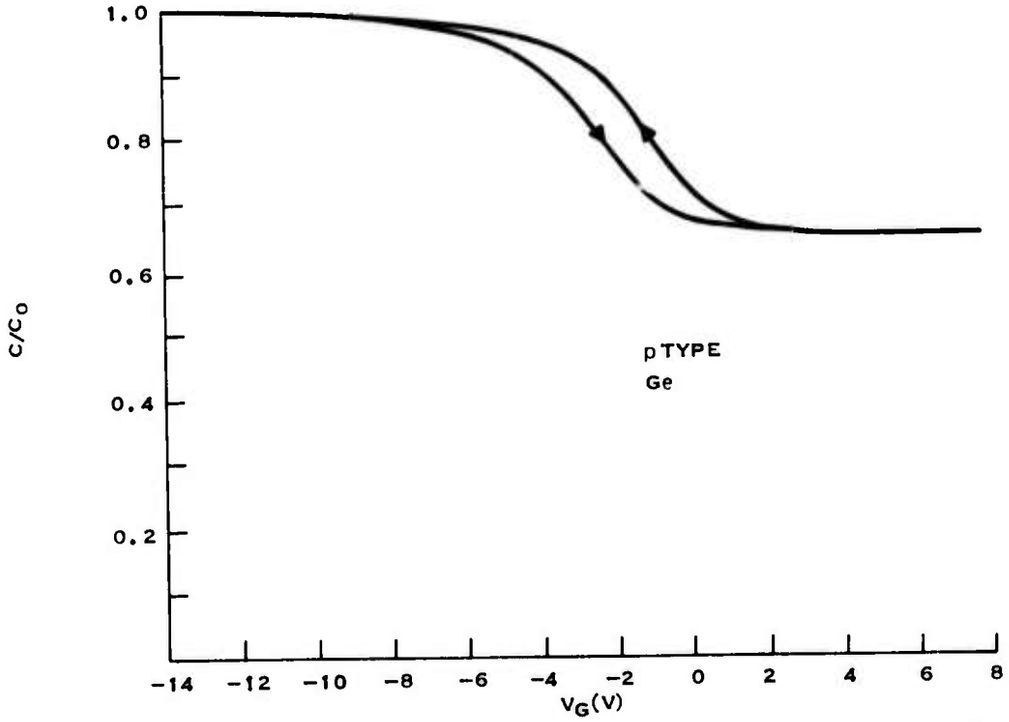

164369

Figure 4-11. Capacitance-Voltage Curve Measured on a Sample Consisting of 1,250 A of RPD SiO_x on Ge of ~3 Ω-cm Resistivity

It follows from Poisson's equation that the flat-band voltage, V_{FB}, is given by

$$V_{FB} = \Phi_{MS} - Q_{SS}\left(\frac{1}{C_{RPD}} + \frac{1}{C_o}\right) - \frac{Q_{S,RPD}}{C_{RPD}} - \frac{1}{C_{RPD}}\int_o^{X_I} \frac{X}{X_I}\,\rho(X)\,d(X) \qquad (4\text{-}7)$$

where Φ_{MS} is the difference between the metal and semiconductor work functions, Q_{SS} and $Q_{S,RPD}$ are the fixed charges at the semiconductor/thermal oxide and thermal oxide/RPD insulator interfaces, respectively, $\rho(X)$ is the charge distribution in the RPD insulator, and X_I is the location of the RPD insulator/thermal oxide insulator thickness. The effect of the last term will depend upon the charge distribution.

A more convenient form for Equation (4-7) is

$$V_{FB} = \left[\Phi_{MS} - \frac{Q_{SS}}{C_o}\right] - \frac{(Q_{SS} + Q_{S,RPD})\,X_I}{K_{RPD}\,\epsilon_o} - \frac{X_I}{K_{RPD}\,\epsilon_o}\int_o^{X_I} \frac{X}{X_I}\,\rho(X)\,d(X) \qquad (4\text{-}8)$$

The bracketed term is the flat-band voltage in the absence of a deposited insulator. The second term depends upon the magnitude of sum of the two surface charges and increases linearly with increasing RPD surface. For this reason, the system chosen for this experiment consisted of a Si wafer which had ~1,000 Å of SiO_2 thermally grown upon the surface to provide a stable interface with a small value of Q_{SS}. The RPD insulator was then grown upon the thermal SiO_2 surface.

Table 4-5 shows the measured flat-band voltage for a series of samples covered with RPD SiN_x and RPD SiO_x as function of time after deposition and RPD insulator thickness. The substrates were ⟨100⟩ n-type Si which had been annealed after growth of the thermal oxide to minimize Q_{SS}. The measured flat band voltage for the thermal oxide alone was −0.6 V.

In the case of RPD SiO_x note that

$$\frac{(Q_{SS} + Q_{S,RPD})\,4{,}000\ \text{Å}}{K_{RPD}\,\epsilon_o} \lesssim -0.5\ \text{V}$$

This implies $(Q_{SS} + Q_{S,RPD})/q \cong 2.5 \times 10^{10}\ /\text{cm}^2$. We know that $Q_{SS}/q \sim 2 - 3 \times 10^{10}\ /\text{cm}^2$; therefore, $Q_{S,RPD}/q \gtrsim 5 \times 10^{10}/\text{cm}^2$.

TABLE 4-5. MEASURED FLAT-BAND VOLTAGE FOR SAMPLES COVERED WITH RPD SiN_x and RPD SiO_x

A (SiN_x)

Thickness \ Storage Time	0 days	8 days	26 days	40 days
1,000 A	>−15	−25	−18	−9
2,000 A	−12	−12	−9	−8
3,000 A	>−15	−15	−10	−5
4,000 A	+4	-	+2	+2

B (SiO_x)

Thickness \ Storage Time	0 days	8 days	26 days	40 days
1,000 A	−1.5	–	−0.8	−0.6
2,000 A	−1	–	−1	−0.5
3,000 A	−1	–	−1	−1
4,000 A	−1	–	−1	−1

The data for SiN_x are quite different from those for SiO_x. Here the initial flat-band voltage could not be measured for two samples because the instrumentation was set up to apply only biases of ±15 V. However, the later temporal behavior of the sample with 1,000 Å of SiN_x may be extrapolated back in time to give $V_{FB} \approx -30$ V at t = o. Ignoring the contribution from the bulk charge in the nitride allows one to calculate that, for SiN_x, $Q_{S,RPD} \cong 6 \times 10^{12}/cm^2$.

It is clear (especially after 40 days) that the flat-band voltage becomes more positive with increasing thickness rather than increasing in the negative direction as Equation (4-7) would predict in the case of no bulk charge. Thus, there must be negative bulk charge present to counteract the positive surface charge. If the bulk charge is assumed to be distributed uniformly with density ρ_o, then integration of Equation (4-7) shows that

$$V_{FB} = \Phi_{MS} - \frac{Q_{SS}}{C_o}$$

when

$$X_1 \rho_o = 2 Q_{S,RPD}$$

Under these assumptions, the bulk charge density in the nitride, $\rho_o \cong 3 \times 10^{17}/cm^3$. There are, of course, not enough data to justify this assumption, but they should give a reasonable estimate until further experiments can provide a more accurate description.

3. Instrumentation

In the first part of the work performed under this contract, electrical characterization of the MIS structures has been limited to capacitance-voltage (C-V) measurements carried out at a single frequency (1 MHz) and dc current-voltage (I-V) measurements. Essentially all of the measurements have been made at room temperature.

This limited characterization has proved sufficient for the initial phases of this work because these measurements provide a good measure of the dc conductance and dielectric constants of the insulator. In addition, the shift in flat-band voltage (hysteresis) under varying applied bias and the voltage rate of change from accumulation to depletion give crude, but quick, estimates of relative magnitudes of mobile insulator and surface charge and fast surface-state density.

However, as Nicollian and Goetzberger[37] point out in their classic paper, while the C-V curve is rich in information concerning surface-state density, extraction of the information from this data is difficult and inaccurate. A better measurement from which to extract information concerning surface-state distribution is ac conductance-voltage (G-V). To maximize the information which can be extracted from this measurement, one would like to do it as a function of frequency and temperature.

C-V and G-V data can be gathered simultaneously by using a phase-locked amplifier to measure the in-phase and quadrature components of the currents through the MIS test structure under the application of an ac voltage. Texas Instruments has chosen to implement such a system using equipment which is commercially available from Princeton Applied Research. Figure 4-12 shows a block diagram of Texas Instruments system and gives the relevant equation for calculating capacitance and conductance.

This system has been assembled together with a probe station which will allow these measurements to be made at a selected temperature in the range ~90°K to ~500°K with cold shielding available at the lower temperatures. In addition to the PAR equipment, a Boonton capacitance meter has been wired into this system to allow quick 1-MHz C-V measurements as well as to provide capability for capacitance versus time (C-t) measurements which give information concerning the dark currents and storage time.

4. Determination of Interfacial-State Densities

The central problem in the extraction of interfacial-state densities from MIS capacitance, capacitance derivative, or conductance data is the theoretical treatment of interfacial charge inhomogeneities. This problem has been discussed extensively[38] and the present situation has been reviewed by Brews.[39] It can be summarized by the statement that the state of the theory is not completely satisfactory and an appeal to experiment is being made to provide further guidance to theoretical development. Experiments designed to attack this problem have apparently been carried out only for the Si-SiO_2 system, however, and even here the data are incomplete.

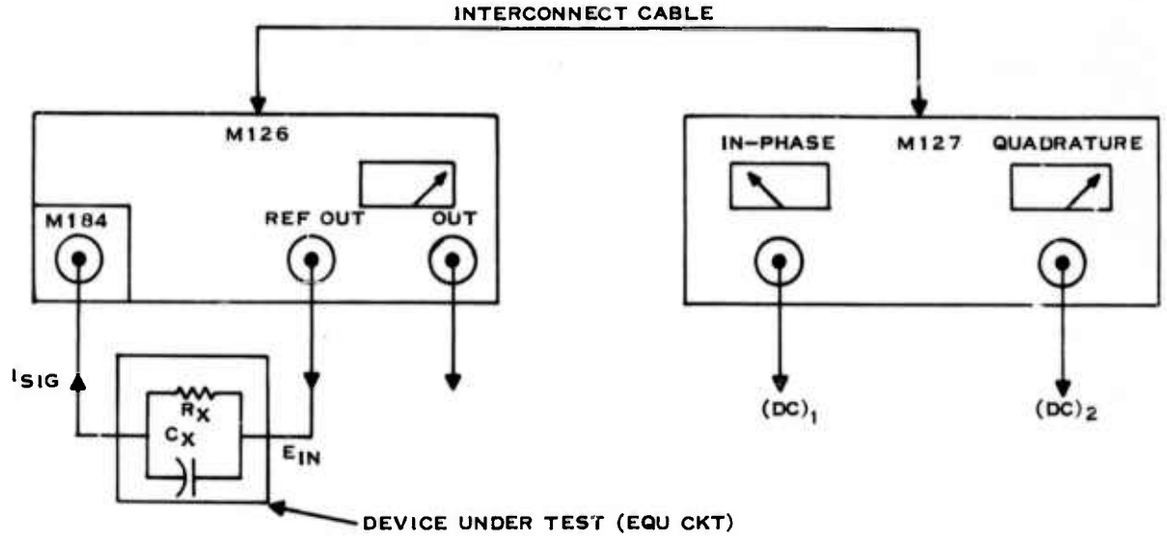

$$\text{A CONDUCTANCE (IN-PHASE)} = R_X^{-1} = \frac{(DC)_{OUT\ 1}}{E_{IN}} \times \frac{V_{FS}}{10} \times \frac{(A/V)}{(PSD)} \text{ MHOS}$$

$$\text{B CAPACITANCE} = C_X = \frac{(DC)_{OUT\ 2}}{E_{IN}} \times \frac{V_{FS}}{10\omega} \times \frac{(A/V)}{(PSD)} \text{ FARADS}$$

DEFINITION OF TERMS

PSD = GAIN EXPANSION OF MIXER/DC AMPLIFIER (X1, 10, OR 100)

164365

Figure 4-12. Block Diagram of the Instrumentation of the New Test Station

Part of the theoretical difficulty lies in the fact that the finite extent of the charge distribution by the carriers at the interface must be taken into account in order to avoid mathematical divergences.[39] This problem cannot be handled classically and must be treated quantum-mechanically. Although it is unlikely that a rigorous theory could be developed under this contract, it should be possible to use some simple quantum-mechanical arguments to further quantify the theory of Brews and thus obtain some reliable estimates of interfacial-state densities as a function of energy for the semiconductor-insulator systems under study here.

SECTION V

CONCLUSIONS AND RECOMMENDATIONS

In the early stages of the contract, the major problem anticipated was the achievement of low interfacial-state densities at the semiconductor-insulator interface. However, there was immediate success in achieving densities of the order 10^{12} cm^{-2} which is low enough to permit control of the interfacial potential by the application of voltage to an electrode on the insulator surface. This degree of success was achieved for the plasma-deposited insulators as well as the liquid-phase-anodized insulators, and at least one of these techniques was successful for all of the semiconductor materials investigated.

However, other disadvantages were found for both of these techniques. The deposited insulators exhibit unacceptably high pinhole densities, even when extreme care in surface preparation and the maintenance of clean conditions is taken, while the liquid-phase-anodized insulators often exhibit low breakdown voltages and high leakage current.

Solutions to these problems may involve a combination of techniques such as anodization followed by plasma deposition; alternatively, the answer may lie in the plasma-anodization technique which Texas Instruments is beginning to explore. These are typical of the insulator fabrication approaches to be taken during the remainder of the contract.

Progress in GaInAs fabrication has been good, and emphasis during the remainder of the contract will be on fabrication of graded epitaxial layers of $Ga_{0.5}In_{0.5}As$.

A much more concentrated effort on the electrical evaluation of the structures is planned for the remainder of the contract, with emphasis on the characterization of interfacial states.

SECTION VI

ACKNOWLEDGEMENTS

Ion backscattering data reported herein were provided by Mr. Joseph Feng of the Department of Electrical Engineering at the California Institute of Technology. AlO_x depositions were performed by Dr. Klaus Wiemer of the Optoelectronics Branch of the Semiconductor Group of Texas Instruments.

REFERENCES

1. T.Y. Wu and G.L. Pearson, *J. Phys. Chem. Solids*, Vol. 33, p. 409 (1972).
2. G.A. Antypas, *J. Electrochem. Soc.*, Vol. 117, p. 1393 (1970).
3. E.F. Hockings, I. Kudman, T.E. Seidel, C.M. Schmelz, and E.F. Steigmeier, *J. Appl. Phys.*, Vol. 37, p. 2879 (1966).
4. J.C. Woolley, C.H. Gillett, and J.A. Evans, *Proc. Phys. Soc.*, Vol. 17, p. 700 (1961).
5. L.G. Bailey, Technical Report AFAL-TR-67-325, Air Force Avionics Laboratory, WPAFB, Ohio, December 1967.
6. H.T. Minden, *J. Electrochem. Soc.*, Vol. 112, p. 300 (1965).
7. R.N. Conrad, P.L. Hoyt, and D.D. Martin, *J. Electrochem. Soc.*, Vol. 114, p. 164 (1967).
8. C.E. Jones, *J. Appl. Spectroscopy*, Vol. 20, p. 161 (1966).
9. A.M. Mearns, *Thin Solid Films* Vol. 3, p. 201 (1969).
10. H.F. Sterling and R.C.G. Swann, *Solid State Electronics*, Vol. 8, p. 653 (1965).
11. M.J. Vasile and G. Smolinsky, *J. Electrochem. Soc.*, Vol. 119, p. 451 (1972).
12. H.R. Phillip, *J. Phys. Chem. Solids*, Vol. 32, p. 1935 (1971).
13. H.R. Phillip, *J. Electrochem. Soc.*, Vol. 120, p. 295 (1973).
14. O. Meyer and W. Scherber, *J. Phys. Chem. Solids*, Vol. 32, p. 1909 (1971).
15. C.J. Dell'Oca, D.L. Pulfrey, and L. Young, *Physics of Thin Films*, Vol. 6, edited by Francombe and Hoffman, Academic Press, N.Y. (1971).
16. L. Young, *Anodic Oxide Films*, Academic Press, New York (1961).
17. D.A. Vermilyea, "Anodic Films," in *Advances in Electrochemistry and Electrochemical Engineering*, Vol. 3, Interscience, New York (1963).
18. "The Birth of the Transistor, an Unforgettable Event," *Electronic Design*, Vol. 20, No. 24, November 23, 1972, p. 69.
19. K.L. Chopera, *Thin Film Phenomena*, McGraw-Hill Book Company, New York (1969), p. 46.
20. L.L. Chang and W.E. Howard, "Surface Inversion and Accumulation of Anodized InSb," *App. Phys. Lett.*, Vol. 7, October 1965, p. 211.
21. J.F. Dewald, "The Kinetics and Mechanism of Formation of Anode Films on Single-Crystal InSb," *J. Electrochem. Soc.*, Vol. 104, p. 244 (1957).
22. B. Schwartz, et al., "The Anodic Oxidation of GaAs in Aqueous H_2O_2 Solution," *Extended Abstracts*, The Electrochemical Society, Vol. 73-1, p. 143 (1973).
23. B. Schwartz and W.J. Sundburg, "Oxidation of GaP in Aqueous H_2O_2 Solution," *J. Electrochem. Soc.*, Vol. 120, p. 576 (1973).
24. R.J. Phelan, Jr. and J.O. Dimmock, "InSb MOS Infrared Detector," *App. Phys. Lett.*, Vol. 10, p. 55 (1967).
25. J.D. Venables and R.M. Broudy, "Anodization of InSb," *J. Electrochem. Soc.*, Vol. 107, p. 296 (1960).

26. W.A. Pliskin, R.G. Simmons, and R.P. Esch, "Infrared Spectra of CO_2 and CO in RF-Sputtered SiO_2 Films," in *Thin Film Dielectrics* (The Electrochemical Society, New York, 1969).

27. J.A. Patterson, A.L. Turkevich, and E. Franzgrote, *J. Geophys. Res.*, Vol. 70, 1965, pp. 1311–1327; A.L. Turkevich, et al., Surveyor Project Final Report, Part 2, Science Results, Jet Propulsion Laboratory Tech. Rep. No. 32-1265, pp. 303–388.

28. J.W. Mayer, L. Eriksson, J.A. Davies, *Ion Implantation in Semiconductors*, pp. 16, 148–176, Academic Press, New York (1970).

29. L. Eriksson, G. Fladda, and P.A. Johansson, Intl. Meeting on Chemical Analysis by Charged Particle Bombardment, Namur, September 1971.

30. R.W. Bower and J.W. Mayer, *Appl. Phys. Letters.*, Vol. 20, 1972, pp. 359–361.

31. J.M. Caywood, *Metallurgical Trans.*, Vol. 4, pp. 735–43 (1973).

32. J.B. Marion and F.C. Young, *Nuclear Reaction Analysis*, (American Elsevier Publishing Co., New York, 1968, p. 154.

33. A.S. Grove, *Physics and Technology of Semiconductor Devices*, John Wiley & Sons Inc., New York, 1967, pp. 278–82.

34. A.M. Mohsen, T.C. McGill, Y. Daimon, and C.A. Mead, *IEEE J. Solid State Circuits*, to be published.

35. J.E. Carnes and W.F. Kosonocky, *RCA Review*, Vol. 33, p. 327 (1972).

36. A.S. Grove, *Physics and Technology of Semiconductor Devices*, John Wiley & Sons, Inc., New York, 1967, pp. 282–5.

37. E.H. Nicollian, and A. Goetzberger, *Belt Syst. Tech. J.*, Vol. 46, p. 1055–1133 (1967.

38. E.H. Nicollian and A. Goetzberger, *Bell System Tech. J.*, Vol. 46, p. 1055 (1967); H. Deuling, E. Klausman, and A. Goetzberger, *Solid State Electronics*, Vol. 15, p. 559 (1972); G.F. Amelio, *Surface Science*, Vol. 29, p. 125 (1972).

39. J.R. Brews, *J. Appl. Phys.*, Vol. 43, p. 2306 (1972).